FANCD2 directly inhibits DNA2 nuclease at stalled replication forks and acts as a RAD51 mediator in strand exchange

Wenpeng Liu[1,5,7], Ivan Roubal[1], Piotr Polaczek[1], Yuan Meng[2,5], Won-chae Choe[1], Marie-Christine Caron[3], Carl A. Sedgeman[1], Yu Xi[5], Changwei Liu[2,5], Qiong Wu[2], Li Zheng[2], Jean-Yves Masson[3,4], Binghui Shen[2], and Judith L. Campbell[1*]

[1] Braun Laboratories, California Institute of Technology, Pasadena, CA 91125, USA

[2] Department of Cancer Genetics and Epigenetics, Beckman Research Institute, City of Hope, 1500 East Duarte Road, Duarte, CA 91010-3000, USA

[3] Genome Stability Laboratory, CHU de Québec Research Center, HDQ Pavilion, Oncology Division, 9 McMahon, Québec City, QC, G1R 3S3, Canada

[4] Department of Molecular Biology, Medical Biochemistry and Pathology; Laval University Cancer Research Center, Québec City, QC, G1V 0A6, Canada

[5] Colleges of Life Sciences, Zhejiang University, Hangzhou, Zhejiang 310027, China

[7]Current address: Department of Biochemistry, Vanderbilt University School of Medicine, 613 Light Hall, 2215 Garland Avenue, Nashville, Tennessee 37232, USA

Correspondence: jcampbel@caltech.edu

Summary

FANCD2 protein, a key coordinator and effector of the interstrand crosslink repair pathway, is also required to prevent excessive nascent strand degradation at hydroxyurea induced stalled forks. The mechanisms of the fork protection are not well studied. Here, we purified FANCD2 to study how FANCD2 regulates DNA resection at stalled forks. In vitro, we showed that FANCD2 inhibits fork degradation in two ways: 1) it inhibits DNA2 nuclease activity by directly binding to DNA2. 2) independent of dimerization with FANCI, FANCD2 itself stabilizes RAD51 filaments to inhibit various nucleases, including DNA2. More unexpectedly, FANCD2 acts as a RAD51 mediator to stimulate the strand exchange activity of RAD51, and does so by enhancing ssDNA binding of RAD51. Our work biochemically explains mechanisms by which FANCD2 protects stalled forks and further provides a simple molecular explanation for genetic interactions between FANCD2 and the BRCA2 mediator.

Introduction

Successful completion of DNA replication requires the integration of many proteins and pathways that protect, repair and/or restart replication forks. The principles underlying how these pathways interact and are regulated to maximize genome stability have yet to be determined. Fanconi anemia is a rare disease of bone marrow failure, developmental abnormalities, and cancer predisposition. At the cellular level it is diagnosed by sensitivity to DNA ICLs (interstrand crosslinking agents) and genome instability. Fanconi anemia is a multigenic disease defined by at least 22 complementation groups, including many regulatory components, nucleolytic activities, and HDR (homology directed repair) genes. The component genes suggest a coherent pathway for maintaining genome stability during DNA replication that goes beyond ICL repair and includes response to many additional types of replication stress(Boisvert and Howlett, 2014; Federico et al., 2018). The multigenic character of the FA pathway lends itself to comprehensive genetic and biochemical dissection(Carr and Lambert, 2013; Chaudhury et al., 2013; Chaudhury et al., 2014; Hashimoto et al., 2010; Kottemann and Smogorzewska, 2013; Lossaint et al., 2013; Petermann et al., 2010; Raghunandan et al., 2015; Schlacher et al., 2011; Schlacher et al., 2012; Sobeck et al., 2006; Yeo et al., 2014).

FANCD2 is a key regulator of the FA pathway and the focus of our current studies(Kottemann and Smogorzewska, 2013; Timmers et al., 2001). During canonical replication-coupled repair of ICLs, after a replication fork encounters an ICL, FANCD2 and a related protein FANCI, are phosphorylated by activated ATR kinase. A FANCD2/FANCI heterodimer is also formed, and FANCD2 in this heterodimer, but not free FANCD2, is mono-ubiquitylated by the FA core complex containing nine FA proteins, including the FANCL E3 ligase complex and several associated proteins. FANCD2-ubi is involved in both activation of repair events and also is directly required in the later enzymatic repair steps at strand breaks

(Knipscheer et al., 2009; Kottemann and Smogorzewska, 2013; Long et al., 2014; Long et al., 2011; Long and Walter, 2012; Raschle et al., 2008). The role of ubiquitin is to enforce stable binding of FANCD2/FANCI to DNA, specifically by clamping FANCD2-ubi/FANCI heterodimers onto DNA for DNA repair(Alcon et al., 2020; Rennie et al., 2020; Tan et al., 2020; Wang et al., 2020).

FANCD2 also appears to have both ubiquitin-independent and FANCI-independent functions. In addition to its role in ICL repair, FANCD2 is required in the BRCA2-regulated, RAD51-mediated replication fork protection pathway, irrespective of the source of DNA damage(Chaudhury et al., 2013; Raghunandan et al., 2015; Schlacher et al., 2011; Schlacher et al., 2012). While several studies of fork protection implied that non-ubiquitylatable FANCD2 (FANCD2-K561R) could not restore fork protection to patient-derived FANCD2-defective cells(Kais et al., 2016; Schlacher et al., 2012), other results support that FANCD2 is likely to have constitutive functions, at least for low levels of replication stress, such as endogenous stress(Boisvert and Howlett, 2014; Federico et al., 2018). With respect to ubiquitylation, study of FANCD2 knockout and knock-in cell lines showed that cells expressing only non-ubiquitylatable FANCD2-K561R had much less severe phenotypes than cells with a FANCD2 knockout (Tian et al., 2017). Complementary studies showed that mutants defective in the trans-acting FA core complex components responsible for ubiquitylation of FANCD2 are less sensitive to replication fork stalling agents than FANCD2 knockdowns or knockouts (Thompson et al., 2017). Importantly, one of us reported that FANCD2 can protect forks by different mechanisms than FANCA/C/G, members of the core complex(Liu et al., 2020). FANCD2 has been shown to interact with RAD51, a key player/regulator in fork protection, and to do so in a ubiquitylation-independent, but HU-stimulated manner(Chen et al., 2017). FANCD2 also has FANCI independent functions(Chaudhury et al., 2013; Dubois et al., 2019; Thompson et al., 2017). FANCD2 deficient cells are HU and aphidicolin (a DNA polymerase inhibitor) sensitive, while FANCI cells are not (Thompson et al., 2017). These results warrant studies of ubiquitin- and FANCI- independent roles of FANCD2.

Fork protection implies protection from nucleases. Several nucleases have been implicated in nascent DNA degradation at stalled forks, in both fork-protection proficient and fork-protection deficient cells (Schlacher et al., 2011; Schlacher et al., 2012; Thangavel et al., 2015). Prominent among these is the DNA2 helicase/nuclease, which seems to play a role in several different fork protection sub-pathways (Liu et al., 2020; Rickman et al., 2020). DNA2 is essential for replication in normal yeast cells(Zheng et al., 2020). Multi-tasking DNA2 removes long 5' ssDNA flaps in the presence of Pif1 helicase during non-canonical Okazaki fragment processing(Budd et al., 2006; Diffley, 2020; Zheng et al., 2020); performs long-range resection of DSBs to provide 3' ends for BRCA2-mediated, RAD51 filament formation and strand invasion during HDR; and prevents deleterious fork reversal in yeast(Hu et al., 2012). At stalled forks, human DNA2 is required for repair of stalled replication forks, where it

mediates limited resection, putatively on a reversed fork, to promote fork restart, in replication fork protection proficient cells(Thangavel et al., 2015). We discovered that DNA2 deficient cells are sensitive to inter- or intra-strand crosslinks induced by cisplatin or formaldehyde. Paradoxically, depletion of DNA2 in cells deficient in FANCD2 rescued ICL sensitivity in FANCD2 mutants, suggesting that DNA2 became toxic in the absence of fork protection(Karanja et al., 2014; Karanja et al., 2012). We and others provided direct evidence that in cells defective in fork protection, DNA2-mediated over-resection occurs at replication forks stalled by exogenous DNA damaging agents or replication inhibition and that FANCD2 is likely to regulate this resection(Higgs et al., 2015; Higgs et al., 2018; Jiang et al., 2015; Liu et al., 2016; Thangavel et al., 2015; Tian et al., 2017; Wang et al., 2015). The question remains as to how FANCD2 regulates DNA2, however. It is not clear if this is direct or indirect because, for instance, RAD51 is also inhibitory to over-resection, apparently through DNA2 inhibition, in vivo(Wang et al., 2015) and because FANCD2 and RAD51 are epistatically linked in fork protection(Schlacher et al., 2012).

Recently, several studies have suggested that FANCD2 and BRCA2 perform parallel or compensatory functions in fork protection and fork recovery after collapse(Kais et al., 2016; Lachaud and Rouse, 2016; Michl et al., 2016). Since BRCA2 is thought to stabilize RAD51 filaments, we hypothesized that FANCD2 may provide a backup source of this BRCA2 function in response to replication stress. This mechanism is supported by the fact FANCD2 alone and FANCD2/FANCI heterodimers interact physically with RAD5(Berti et al., 2013; Chen et al., 2017; Sato et al., 2016; Thangavel et al., 2015; Thangavel et al., 2010). FANCD2/FANCI complexes have been shown to increase RAD51 levels on DNA, but the specific contribution of FANCD2 itself and the relationship of this observation to suppression of BRCA2$^{-/-}$ defects has not been established.

In this work we delved deeper into the mechanisms of FANCD2 fork protection by comparing the effect of FANCD2 deficiency on replication forks stalled due to acute or chronic replication stress induced by different damaging agents. Our in vivo results confirm that FANCD2 is required to protect stalled replication forks from DNA2-dependent over-resection after acute stress. They also revealed, however, that FANCD2 has an additional and opposing function that is needed for promoting resection after prolonged stress. We identified at least two potential mechanisms by which FANCD2 protects nascent DNA from nucleolytic resection in vitro: 1) FANCD2 inhibits DNA2 nuclease activity and binds directly to the DNA2 nuclease domain; and 2) FANCD2 stabilizes RAD51 ssDNA filaments which prevent nucleolytic digestion by multiple nucleases. Surprisingly, we also find that FANCD2, like BRCA2, acts as a mediator in RAD51-dependent strand exchange. FANCD2 promotes RAD51 mediated strand exchange activity by stabilizing RAD51 on ssDNA, but not, like BRCA2 by inhibiting the RAD51 ATPase or RAD51 dsDNA binding activities, and not requiring FANCD2 DNA binding motifs. All the in vitro activities of FANCD2 are FANCI independent and interaction with DNA2

is ubiquitin independent in vitro. The ability to stimulate strand exchange adds a novel mechanistic explanation for the well-documented dependency of BRCA2$^{-/-}$ tumors on FANCD2, the suppression of BRCA1/2$^{-/-}$ phenotypes by elevated levels of FANCD2(Kais et al., 2016; Lachaud and Rouse, 2016; Michl et al., 2016), and adds a new dimension to how FANCD2 deficiency leads to inhibition of fork protection and genome instability(Schlacher et al., 2012).

Results

FANCD2 Plays Different Roles in Repair at Different Extents/Stages of Fork Stalling

FANCD2 has been demonstrated by iPOND to associate with replication forks, and to increase four to five fold in the presence of HU(Dungrawala et al., 2015). To further verify the association of FANCD2 with replication forks stalled by HU, we labeled nascent DNA strands with the thymidine analog BrdU in the presence of HU under conditions that specifically mark nascent ssDNA (single-stranded DNA) and used immunofluorescence to monitor localization of FANCD2 and γH2AX(Couch et al., 2013). We find that γH2AX foci and FANCD2 foci co-localize with BrdU-marked nascent ssDNA foci (Figure 1A). We then compared the level of association of FANCD2 with replication forks in the absence and presence of HU by immunofluorescence (see Method Details). We detected FANCD2/EdU associated foci only after HU treatment (Figure 1B). (Note that the images were magnified and the ratio of cells with >4 FANCD2/EdU colocalized foci to total cells was determined). The difference between IPOND and immunofluorescence (IF) in observed FANCD2 association with the nascent DNA in the absence of HU may be due to assay detection resolution. We conclude that FANCD2 substantially recruited to stalled replication forks in the presence of HU.

Multiple pathways are involved in stalled replication fork repair, and forks undergo sequential changes in architecture during chronic stalling(Helleday et al., 2008; Lemacon et al., 2017; Petermann et al., 2010; Quinet et al., 2017). A major question in FANCD2 mediated repair is what structure is being acted upon and whether this substrate changes during the course of fork pausing and processing(Petermann et al., 2010; Piberger et al., 2019). To investigate this question, we monitored resection in FANCD2 deficient cells at various extents of stalling with either HU, CPT (camptothecin), or cisplatin, each of which induces a different type of replication stress. Initially we used RPA2 phosphorylation as a surrogate for measuring ssDNA arising during resection in the presence of HU. Cells were treated with HU for 0-8 h and nuclear extracts prepared. At all-time points, we observe drastically increased RPA-p levels (resection) in nuclear extracts of HU-treated PD20 FANCD2$^{-/-}$ deficient cells compared to PD20:FANCD2 (FANCD2-complemented) cells, where there was very little resection (Figure 1C). This is consistent with other published results showing that FANCD2 protects stalled forks from nascent DNA degradation. Unexpectedly, however, we see a change in the pattern over the time course. In PD20 cells, we observe an initial increase in resection at early

times, 2-4 h of treatment, but then a decline in resection with treatment up to 8 h, though there is still substantial over-resection. We interpret the decline of RPA-p at later times in the continued presence of HU as due to conversion of the initial, RPA-p marked damage that is protected by FANCD2, into other lesions, such as DSBs or gaps (collapse) and that FANCD2 is required for resection of the latter structures. A change in structure is supported by neutral COMET assay (Figure S1A). The proposed requirement for FANCD2 on fork collapse is consistent with the fact that FANCD2 tethers CtIP to collapsed forks, and CtIP stimulates resection needed for repair after extensive ICL-induced stalling(Murina et al., 2014; Unno et al., 2014; Yeo et al., 2014), either by recruitment and stimulation of BLM and DNA2 nuclease to resect the end of the break(Ceppi et al., 2020; Hoa et al., 2015; Yeo et al., 2014), or by recruitment of pol theta and stimulation of alternative non-homologous end joining (alt-NHEJ)(Badie et al., 2015; Zhang and Jasin, 2011).

The proposal that FANCD2 can have two opposing effects on resection is also supported by the fact that PD20 cells treated with CPT (camptothecin) behave differently from those treated with HU (Figure 1D). While CPT can also induce fork slowing or stalling(Ray Chaudhuri et al., 2012), it rapidly induces DSBs when the replication fork encounters sites of the CPT-induced Top1-DNA cleavage complexes(Berti et al., 2020; Whelan and Rothenberg, 2021). We do not see an overall increase in resection after CPT treatment in the absence of FANCD2 in the PD20 cells compared to the complemented cells (Figure 1D and Figure S1C), which we attribute to the dominance of DSB lesions that require FANCD2 for resection. We do still see that in the absence of FANCD2, there is over-resection at early times compared to later times (Figure 1D, lanes 3 and 4 compared to lanes 5 and 6) in PD20 cells, similar to HU, suggesting there is some fork stalling at earlier times with fork collapse after chronic exposure, as with HU(Berti et al., 2020; Whelan and Rothenberg, 2021). We obtained supporting data for the difference in replication fork structure caused by HU and CPT using neutral COMET assays. In HU, after mild treatment, there is a low level of DSBs that increase as the extent of HU treatment is increased (Figure S1A). With CPT, there is a greater level of DSBs at early times and they increase rapidly and extensively with prolonged treatment (Figure S1B).

Cisplatin treatment phenocopies CPT since RPA2-p in FANCD2-deficient cells prepared by knockdown of FANCD2, is significantly decreased after prolonged treatment with either compound (Figure S1D). Comparison of the results with HU to those with CPT suggests that transiently stalled, possibly reversed replication forks, rather than DSBs, are the primary sites of FANCD2 negative regulation of resection and that different repair mechanisms may function on CPT and cisplatin damage, as recently proposed by others(Couch et al., 2013; Rickman et al., 2020).

In summary, our results suggest that FANCD2 is required to protect from over-resection at early times after damage on forks transiently stalled by HU. FANCD2, however, may play a different role during chronic stalling that leads to fork collapse to DSBs or to other types of

damage, when it may actually be required for resection and repair.

FANCD2-mediated Regulation of End Resection Occurs on Nascent DNA upon Replication Stress

To more directly investigate replication fork-coupled resection in FANCD2-deficient cells, we next used single molecule tracking of nascent DNA before and after brief (4h) HU treatment. As reported previously, we see over-resection in the FANCD2 depleted cells, just as we saw using RPA-p as the readout for resection (Figure 1C). The resection we observe might occur either on single-stranded “flaps” on uncoupled forks, on forks with gaps due to re-priming, or on the regressed arm of reversed forks(Piberger et al., 2019; Quinet et al., 2019; Zellweger et al., 2015). Regressed forks arise when forks stall, template strands rewind, and nascent strands anneal, forming a four-way junction similar to a Holliday junction(Higgins et al., 1976). Zellweger et al. demonstrated that both uncoupled forks with gaps and reversed forks accumulate in cells treated with low levels of HU(Zellweger et al., 2015). To test the model that over-resection in FANCD2-deficient cells occurred on reversed forks, we monitored resection in FANCD2-depleted cells and in cells co-depleted for FANCD2 and RAD51, the SMARCAL1 translocase or ZRANB3 translocases, all of which have been reported to mediate HU-induced fork reversal and to be required for fork degradation in the absence of the FA/BRCA fork protection pathway(Betous et al., 2013; Bhat et al., 2015; Couch et al., 2013; Kolinjivadi et al., 2017b; Lemacon et al., 2017; Mijic et al., 2017; Taglialatela et al., 2017; Vujanovic et al., 2017; Zellweger et al., 2015). We find that co-depletion of either RAD51 or SMARCAL1 or ZRANB3 with FANCD2 resulted in significant rescue of over-resection (Figure 2A and 2b). Similar results were obtained with BRCA2 knockdowns (Figure 2B),as reported by numerous studies. The results suggest that the over-resection upon limited HU treatment in FANCD2 deficient cells occurs primarily on reversed fork substrates. Furthermore, both SMARCAL1 and ZRANB3 are likely required to produce the substrate since knockdown of either one completely protected from observable nascent DNA degradation.

We also monitored the effect of SMARCAL1 and ZRANB3 on resection after CPT treatment using the RPA-p western blot assay. Knockdown of SMARCAL1 slightly reduced resection but ZRANB3 siRNA did not after CPT treatment (Figure S2A). Co-depletion of FANCD2 and FANCM, another factor capable of reversing forks in vitro, also reduced resection (Figure S2A). However, we see more residual resection after ZRANB3 depletion in the assays for RPA-p after CPT treatment (Figure S2A) than we see in the DNA fiber experiment after HU treatment (Figure 2B), supporting our proposal that reversed fork structures may not be the sole substrates for resection after CPT treatment. Thus, the RPA-p assay may also be detecting resection at forks collapsed to DSBs when the fork encounters the single-strand break induced by CPT treatment (or at non-specific DSBs) rather than after

decay of a reversed fork substrate that failed to be repaired or at gaps behind the fork(Hashimoto et al., 2010). CPT damage may have different requirements for restart, consistent with the difference in the level of resection after CPT treatment compared to results with HU (Figure 1C and 1D).

MUS81 and SLX1/4 are structure specific endonucleases that can cleave unrepaired, long-lived reversed forks such as arise at an ICL or after prolonged fork stalling by other agents, to produce DSBs. To directly test if such DSBs were substrates for over-resection, we co-depleted FANCD2 and MUS81 or SLX4 to see if knockdown could reduce HU-induced fork degradation (Figure 2C). Depletion of MUS81 and SLX4 did not affect the HU-induced nascent degradation observed in the absence of FANCD2, supporting that the fork degradation detected in the absence of FANCD2 by fiber tracking is not due to previous endonucleolytic digestion (by these nucleases) but rather by resection of reversed forks.

DNA2 or MRE11 Depletion Reverses the Over-resection of Nascent DNA in the Absence of FANCD2 upon Replication Stress

Following up on our observation that knockdown of DNA2 can rescue the cisplatin and formaldehyde sensitivity of the FANCD2$^{-/-}$ PD20 patient cell line(Karanja et al., 2014), we confirm that degradation of nascent DNA in FANCD2-deficient cells upon HU treatment can be rescued by knockdown of DNA2 but also by knockdown of MRE11 nuclease (Figure 2D and Figure S2B), just as knockdown of DNA2 significantly decreases this RPA-p, i. e. resection, in cisplatin treated FANCD2$^{-/-}$ cells with brief cisplatin treatment (Figure S2C, lane 4). MRE11 and DNA2 may function as alternative nucleases or function sequentially, as they do at DSBs (Symington and Gautier, 2011). We also tested the role of DNA2 after brief CPT treatment using the RPA-p assay; the results show that DNA2 but not CtIP knockdown reverses the over-resection in the absence of FANCD2 upon short CPT treatment (Figure S2D and S2E). In the presence of FANCD2, knockdown of CtIP reduces resection, consistent with an important role for FANCD2 mentioned above in CtIP recruitment and the ability of CtIP to stimulate both MRE11 and WRN/BLM-DNA2 mediated resection in vitro(Ceppi et al., 2020).

The difference between MRE11 and CtIP in the absence of FANCD2 is consistent with 2-D gel studies in yeast that show that Sae2, the CtIP ortholog, only participates in resection at late collapsed forks and not at early reversed-fork or uncoupled-fork intermediates(Colosio et al., 2016). They are also consistent with our proposal that the requirement for FANCD2 after chronic exposure to HU occurs at collapsed rather than reversed forks.

DNA2 Depletion Can Rescue Replication Restart Defects Observed in the Absence of FANCD2

We next tested if the over-resection leads to replication restart defects such as are found in aphidicolin treated FANCD2 deficient cells(Yeo et al., 2014). We performed DNA combing assays to determine stalled fork restart efficiency after HU or cisplatin treatment (Figure S2F). We found that restart efficiency is moderately decreased in FANCD2 or DNA2 knockdown in U2OS cells, consistent with previous studies(Yeo et al., 2014). However, combining DNA2 and FANCD2 knockdown in U2OS cells rescues the restart defects in both HU and cisplatin treatment. These results reveal that nascent strand degradation in FANCD2 deficient cells can reduce restart efficiency, and that rescue of nascent DNA degradation by depleting DNA2 restores restart efficiency.

FANCD2 Inhibits DNA2 Nuclease Activity in vitro Providing a Mechanism for FANCD2's in vivo Role at Reversed Forks

Since over-resection in PD20 cells treated with HU is massively increased over the FANCD2-complemented cells at all extents of treatments (Figure 1C), and since FANCD2 and DNA2 have been shown to interact in vivo in a DNA-independent fashion, suggesting a protein/protein interaction(Karanja et al., 2012), we tested whether FANCD2 directly regulates degradation by DNA2 nuclease. FANCD2-His was purified from SF9 insect cells (Figure S3A)(Roques et al., 2009) and was shown bind to dsDNA (Figure S3B) and to be free of nuclease activities under the conditions used here (Figure 3A). When FANCD2 was added to a DNA2 nuclease reaction, significant inhibition of DNA2 nuclease was observed, even in the presence of high levels (5 nM) of DNA2 (Figure 3B and Figure S3C). Inhibition is likely due to FANCD2 protein since all reactions contained the same amount of FANCD2 diluent. In these experiments, the substrate partially mimics a stalled replication fork with single-stranded DNA arms at the dsDNA junction. DNA2 processes substrates with several different configurations, such as unligated 5' flaps on Okazaki fragments or on base excision repair intermediates, or 5' overhangs on regressed replication forks during replication fork stress/stalling or during DSB resection during homologous recombination. As shown in Figures 3C and 3D and Figure S3C, FANCD2 inhibits DNA2 nuclease on each of these structures. (Sequences of all oligonucleotide substrates used are provided in Table S2. The substrates mimicking reversed fork DNAs with or without a 5' overhang (Figure 3D) were generated and validated as described in Figure S3D).

FANCD2 forms stable complexes with FANCI in vivo and in vitro, although only 20% of the FANCD2 in the cell co-IPs with FANCI(Alcon et al., 2020; Tan et al., 2020). We also tested if FANCI inhibited DNA2 and showed that there was no inhibition of DNA2 nuclease, except at the highest FANCI concentrations (Figure 3E). When FANCI was added along with FANCD2, the small amount of nuclease activity remaining after inhibition of DNA2 by FANCD2 was not further inhibited by FANCI (Figure 3F).

We next addressed the specificity of FANCD2 inhibition for DNA2. Since depletion of MRE11 suppressed the nascent DNA degradation in FANCD2 knockdowns (Figure 2D), we tested the ability of FANCD2 to inhibit MRE11. MRE11 activity on duplex DNA was inhibited by FANCD2, also consistent with a protein/protein interaction(Roques et al., 2009) (Figure 3G). We also tested the effect of FANCD2 on EXO1 (Figure 3H). EXO1 was not inhibited by FANCD2, so there is specificity to the inhibition of MRE11 and DNA2 by FANCD2.

How Does FANCD2 Inhibit DNA2 Nuclease?

We next asked whether inhibition was mediated by a DNA2/FANCD2 protein/protein interaction and/or by a FANCD2 protein/DNA interaction. We purified His-tagged hFANCD2 from *E. coli* and FLAG-tagged hDNA2 protein from human cells as described in Method Details(Takahashi et al., 2014) (Figure 4A). Immunoprecipitation experiments show that purified DNA2 and FANCD2 bind directly and strongly to each other (Figure 4B and 4C) and that the interaction is independent of DNA (Figure 4D), further supporting that in vivo interaction may also be direct, consistent with our previous finding that DNA2 and FANCD2 also reciprocally coIP in extracts of CPT-treated cells and that the interaction is independent of DNA(Karanja et al., 2012).

Using site-directed mutagenesis we identified a region on DNA2 in the N terminus spanning a.a (amino acid) 227 to 348 that severely reduces coimmunoprecipitation with full-length FANCD2 (Figure 4E and Methods). This region includes the canonical DEK nuclease family active site motifs(Budd and Campbell, 2000; Yang, 2011), suggesting how the interaction might interfere with nuclease function. We next used a complete set of fragments of FANCD2 to determine the region that inhibits DNA2, a functional assay for “interaction”. As shown in Figure 4F, fragment F1, a.a. 1-588 was the only sub-fragment that inhibited DNA2. This region contains the FANCD2 ubiquitylation site (a.a. K561), and addition of a ubiquitin coding sequence to F1 fragment, designated F1-ubi, increased the efficiency of inhibition. These results imply that a protein/protein interaction is needed to inhibit DNA2 nuclease activity.

We also investigated whether DNA binding by FANCD2 was involved in the inhibition of DNA2. To do so, we used FANCD2-F1+F3Mut, which is defective, though not completely blocked, in DNA binding (Figure S4A and S4B)(Niraj et al., 2017). Like WT FANCD2, FANCD2-F1+F3Mut showed no nuclease activity itself (Figure 4G, controls, left) and strongly inhibited DNA2 nuclease on the fork structure (Figure 4G, right) and with only marginally reduced potency on the reversed fork structures (Figure 4H), although it bound to ssDNA 10-fold less efficiently than WT FANCD2 (Figure S4B), consistent with previous characterization of the FANCD2-F1+F3Mut protein(Niraj et al., 2017). This suggests that direct protein/protein interaction contributes to DNA2 inhibition and that inhibition does not occur by simply blocking the substrate or competing with DNA2 for the substrate.

Since the FANCD2-F1+F3Mut protein showed residual binding to DNA, however, to further test whether DNA2 inhibition is through a protein/protein interaction, we investigated whether inhibition by FANCD2 is species-specific. Yeast lacks a FANCD2 ortholog, and we hypothesized that yeast DNA2 would only be inhibited by FANCD2 if inhibition was mediated by occlusion/sequestration of DNA, thus preventing binding by DNA2. We observed no inhibition of yeast DNA2 by FANCD2, even at great molar excess FANCD2, on either the forked substrate or the reversed fork substrate (Figure S4C and S4D). Note that yDNA2 is more active than hDNA2, as also reported by others(Kumar et al., 2017), accounting for the concentrations used. The lack of inhibition of yeast DNA2 by FANCD2 supports, though it does not prove, that inhibition of hDNA2 by FANCD2 involved a species-specific and therefore likely a physiologically significant protein/protein interaction.

DNA2 is also Inhibited by RAD51 Filaments

In addition to rescue by DNA2 nuclease depletion or specific chemical inhibition of nucleases, failure of BRCA2 or FANCD2 fork protection and resulting nascent DNA degradation has been shown to be rescued by elevated RAD51 levels or by stabilization of RAD51 filaments(Bhat et al., 2018; Schlacher et al., 2012; Wang et al., 2015). Furthermore, FANCD2 and RAD51 show epistatic interaction in nascent DNA degradation assays, i.e. destabilization of RAD51 filaments does not lead to further degradation of nascent DNA in FANCD2 deficient cells(Schlacher et al., 2012) and see also(Hashimoto et al., 2010; Hashimoto et al., 2012; Higgs and Stewart, 2016; Kolinjivadi et al., 2017b; Schlacher et al., 2011; Schlacher et al., 2012; Taglialatela et al., 2017; Thangavel et al., 2015; Wang et al., 2015; Zadorozhny et al., 2017). To explore potential molecular interplay between FANCD2 and RAD51 in regulating DNA2-mediated resection, we first looked at whether there is physical interaction between DNA2, RAD51, and FANCD2 in HU-treated cells. We show that RAD51 co-IPs with FLAG-DNA2 and with endogenous FANCD2 (Figure 5A). Reciprocally, we immunoprecipitated RAD51 and showed that both FANCD2 and endogenous DNA2 coimmunoprecipitated (Figure 5B). The RAD51 immunoprecipitation in Figure 5B, which was analyzed under different gel conditions from the α-FLAG-DNA2 IP in Figure 5A, reveals that both mono-ubiquitylated and non-ubiquitylated FANCD2 are present in the co-immunoprecipitates. We then repeated these experiments after treating extract with Benzonase (Figure 5C). The RAD51/FANCD2 interaction was still observed (Figure 5C) and is therefore not dependent on DNA, in keeping with previous observations(Sato et al., 2016). However, since RAD51 was not found in a DNA2 IP after treatment of extracts with Benzonase (Figure 4D), we conclude the interaction of DNA2 with RAD51 requires DNA and is not direct.

Although DNA2 and RAD51 don't appear to interact directly, RAD51 filaments have been implicated in regulating DNA2-mediated resection(Wang et al., 2015). We tested for inhibition of FLAG-DNA2 nuclease by recombinant RAD51 protein. To distinguish between inhibition by RAD51 protein alone and inhibition by RAD51 filament formation, we took advantage of the

demonstration that Ca^{2+} permits filament formation but modulates ATP hydrolysis and inhibits dissolution of the filaments, resulting in stabilization(Bugreev and Mazin, 2004). As shown previously and in Figure 5D, RAD51 filaments can be formed in the presence of ATP and are more stable in the presence of Ca^{2+} than in its absence (compare lanes 2 and 4 and lanes 10 and 12, Figure 5D). We then determined the effect of increasing amounts of RAD51 on DNA2 nuclease activity. As shown in Figure 5E and 5F, RAD51 inhibits DNA2 degradation in the presence of Ca^{2+} but inhibits much less in the absence of Ca^{2+}, where filaments are less stable. The Ca^{2+} effect suggests that inhibition is due to RAD51 filaments. RAD51 also inhibits DNA2 on forked and 5'-flap substrates (Figure 5G and 5H). RAD51 filament stabilization might block many nucleases [Figure S5A and (Kolinjivadi et al., 2017b)], bringing into question the physiological significance of RAD51 inhibition of DNA2. Therefore, we turned our attention to the study of additional functions for RAD51 and FANCD2 interaction in fork protection.

FANCD2 Stimulates Strand Exchange by High Concentrations of RAD51

We were struck by the fact that $BRCA2^{-/-}$ cells and $FANCD2^{-/-}$ show non-epistatic interactions such as synthetic lethality and that over-expression of FANCD2 suppresses $BRCA^{-/-}$ phenotypes(Kais et al., 2016; Michl et al., 2016). Furthermore, like BRCA2, FANCD2 interacts physically and robustly with RAD51 [Figure 5 and (Chen et al., 2017; Sato et al., 2016)], and RAD51 has been shown to localize to stalled forks in cells lacking BRCA2(Kolinjivadi et al., 2017b). We hypothesized that FANCD2 might, similarly to BRCA2, stimulate RAD51-mediated strand exchange(Jensen et al., 2010; Thorslund et al., 2010). While FANCD2 does not enhance RAD51-mediated D-loop assays with resected plasmid substrates(Dubois et al., 2019), complete strand exchange assays with oligonucleotides were never tested. Both reactions are linked to DNA recombination, but mechanistically they are different. In D-loop assays strand invasion into a supercoiled DNA recipient is measured and is thought to represent a search for homology(Carreira et al., 2009; Carreira and Kowalczykowski, 2011). Strand exchange assays, in contrast, measure a complete transfer of DNA strands (see schematic in Figure 6A). As indicated, RAD51 catalyzes the exchange of the labeled strand in the duplex to ssDNA to form the strand exchange product(Jensen et al., 2010; Thorslund et al., 2010). High concentrations of RAD51, however, have been shown to be inhibitory in this assay(Jensen et al., 2010; Thorslund et al., 2010). To measure strand exchange, RAD51 was incubated, in the presence or absence of FANCD2, with unlabeled ssDNA (Figure 6B, pilot experiment), with duplex DNA with a 3' ssDNA overhang (Figure 6C), or with duplex DNA with a 5' ssDNA overhang (Figure 6C) to allow filament formation. Fully duplex DNA containing a ^{32}P labeled strand complementary to the ssDNA or respective overhang DNA was then added. Stimulation of strand exchange by RAD51 is shown for ssDNA in Figure 6B, lanes 1-4. Inhibition at high RAD51 levels is shown in Figure 6B, lane 5. Such inhibition is proposed to arise once ssDNA is saturated with RAD51, allowing the excess RAD51 to bind to the labeled

dsDNA donor, which inhibits exchange(Jensen et al., 2010; Thorslund et al., 2010). Supporting the hypothesis that the inhibition by high levels of RAD51 can be due to binding of excess RAD51 to duplex DNA, we showed that addition of a dI-dC oligonucleotide relieves inhibition, presumably by successfully competing with the labeled duplex donor for excess RAD51 binding in the assays (Figure 6B, lane 12). We then studied whether FANCD2 stimulated RAD51 at high RAD51 concentrations, as has been shown for BRCA2(Jensen et al., 2010; Thorslund et al., 2010). As shown in Figure 6B (lanes 6-11) and Figure 6C, although FANCD2 has no strand exchange activity on its own, FANCD2, indeed, reproducibly stimulates strand exchange by high concentrations of RAD51 and does so in a concentration dependent manner. Strand exchange involving duplex DNA with a 3' or 5' overhang, more closely resembling a filament on resected DNA, was stimulated more efficiently than with ssDNA, suggesting that stimulation may occur on DNA with ds/ss junctions and may occur at gaps as well as at ssDNA tails (Figure 6B, C). Several controls that strand exchange was occurring were performed. Reversing the order of addition of substrates, i.e., formation of RAD51 filaments on dsDNA and then addition of ssDNA, did not lead to exchange (Figure S6); thus, we are not observing inverse strand exchange(Mazina et al., 2017). Addition of cold oligonucleotide to the stop reaction does not change the products, supporting that the strand exchange products are not formed due to denaturation and renaturation in the stop mixture (Figure 6C, lanes labeled cold oligo)(Jensen et al., 2010). We conclude that FANCD2 stimulates RAD51 mediated strand exchange.

We next interrogated the mechanism of FANCD2 stimulation of RAD51. BRCA2 DNA binding is required for stimulation of strand exchange, and BRCA2 is thought to stimulate strand exchange in several ways: by stabilizing RAD51 filaments through inhibiting RAD51 DNA-dependent ATPase, by promoting the handoff of ssDNA from RPA to RAD51, and by nucleating filament formation on ssDNA while inhibiting filament formation on duplex DNA. To determine if FANCD2 DNA binding was required for stimulation of strand exchange, we tested if the FANCD2 DNA binding mutant described above stimulated strand exchange(Niraj et al., 2017). Although FANCD2-F1+F3Mut showed approximately ten-fold reduction in ssDNA binding at 10 nM (Figure S4B), FANCD2-F1+F3Mut protein stimulates strand exchange even more efficiently than FANCD2 WT (Figure 6D). We next determined if FANCD2 inhibits RAD51 DNA-dependent ATPase. Surprisingly, unlike BRCA2, FANCD2 does not inhibit RAD51 DNA-dependent ATPase (Figure 6E), and thus may not be acting to stabilize RAD51/ssDNA filaments by blocking the ATPase.

We finally tested if FANCD2 plays a role in targeting RAD51 preferentially to ssDNA by inhibiting nucleation on dsDNA. We carried out DNA binding experiments using biotin-streptavidin pull-downs (Figure 6F). We first demonstrated that dsDNA inhibits RAD51 binding to a biotin-labeled 3' overhang substrate (Figure 6G). We then added FANCD2 and found that FANCD2, unlike what has been demonstrated for BRCA2, which has been shown to

specifically overcome dsDNA inhibition of RAD51 binding to overhang DNA(Jensen et al., 2010; Thorslund et al., 2010), did not stimulate association of RAD51 with the 3' overhang substrate in the presence of excess dsDNA (Figure 6H). Thus, FANCD2 is not stimulating RAD51 by reducing binding to dsDNA and is more likely stabilizing RAD51/ssDNA filaments. Supporting this interpretation, FANCD2 does stimulate the accumulation of RAD51/ssDNA complexes in the absence of dsDNA (Figure 6I), consistent with previous characterization of RAD51/FANCD2/FANCI interaction with DNA(Sato et al., 2016). In summary, we suggest that FANCD2 stimulates strand exchange by directly promoting, either through nucleation, assembly, or filament stabilization, RAD51/ssDNA filament formation, rather than by competing with dsDNA. This FANCD2-mediated stabilization does not involve inhibition of RAD51 ATPase and does not require optimum FANCD2 DNA binding activity. Stimulation of strand exchange with these characteristics suggests that the molecular role of FANCD2 in fork protection and restart may involve stimulation of formation of or stabilization of RAD51 filaments in addition to the direct inhibition of DNA2 shown in Figure 4. The results further suggest that interaction of FANCD2 with RAD51 protein [Figure 5 and(Sato et al., 2016)] contributes to strand exchange, and therefore that this may contribute to the ability of elevated levels of FANCD2 to suppress some BRCA2-deficiencies(Ceccaldi et al., 2015; Michl et al., 2016).

Discussion

FANCD2 has been studied for decades and much has been learned about its cellular and structural. What is unknown, however, despite extensive cellular and structural characterization, are the biochemical activities it uses to accomplish and coordinate its diverse in vivo roles. During our studies of cellular responses to DNA replication stress and maintenance of genome stability, our work on the DNA2 helicase/nuclease, a protein involved in resection necessary for replication fork protection, confirmed that FANCD2 regulates DNA2 resection. This led us to undertake a biochemical reconstitution of study of stalled fork resection to identify the important biochemical functions of DNA2, i.e. resolution and reconstitution. A model summarizing our results is shown in Figure 7.

Two Opposing Roles for FANCD2 at Stressed Replication Forks

In pursuing the discovery that FANCD2 and DNA2 show synthetic viability in the presence of ICLs, we now demonstrated that over-resection of nascent DNA that occurs in FANCD2 deficient cells after brief replication stress induction by either HU, CPT or cisplatin, is suppressed by depletion of DNA2, correlating with the cisplatin resistance of FANCD2/DNA2 doubly deficient cells, consistent with other recent reports(Higgs et al., 2018; Rickman et al., 2020). We further demonstrate, for the first time, however, that after HU treatment this over-resection occurs on stalled forks reversed by SMARCAL1 and ZRANB3 as well as RAD51 (Figure 2). DSBs do not seem to be a substrate for DNA2 hyper-resection in the absence of

FANCD2 since SLX4 and MUS81 are not required for nascent DNA degradation during short HU treatment.

Unexpectedly, we found that this DNA2-inhibitory function of FANCD2 is only observed at low levels of replication stress. In contrast, with chronic, or more extensive replication fork stress, we find that FANCD2 is required for resection, rather than inhibiting it. To explain the difference between short and extended HU, and between HU and CPT in FANCD2 deficient cells, we propose that during extended HU treatment, the stalled replication forks progressively accumulate structures such as gaps due to fork uncoupling/repriming or DSBs due to fork collapse (Figure 7). These structures require FANCD2 for resection, which is, in turn essential for their repair by post-replication mechanisms(Cong et al., 2019; Lemacon et al., 2017; Panzarino et al., 2019; Petermann et al., 2010; Piberger et al., 2019; Quinet et al., 2019; Ray Chaudhuri et al., 2015). Indeed, FANCD2 was previously shown to stimulate resection at forks stalled by ICLs for 24 h by recruiting CtIP(Murina et al., 2014; Unno et al., 2014; Yeo et al., 2014). CtIP may be involved in HR and/or to recruit pol theta to promote resection for alt-NHEJ(Kais et al., 2016). We suggest that we are detecting a similar function for FANCD2, that is stimulation of resection specifically at HU stalled forks that fail to be repaired during fork reversal and that progress into collapse or restart (Figure 7). A similar model applies to CPT-treated cells, but the requirement for FANCD2 for repair is much more prominent, since DSBs are the primary fork damage and much more rapidly induced by the Top1/DNA cleavage complexes when they are encountered by progressing replication forks than they are by HU (Figure 7, CPT).

FANCD2 Inhibits DNA2 in vitro

To address this complexity, we undertook to reconstitute FANCD2-dependent reactions with purified proteins. We then showed that FANCD2 protein mediates direct inhibition of the resection activity of DNA2 nuclease, uncovering a molecular mechanism for how FANCD2 mediates fork protection at reversed forks at low level of stress. We find that mutant FANCD2 protein that is defective in DNA binding inhibits DNA2 as well as wild-type FANCD2. Furthermore, since FANCD2 does not inhibit yeast DNA2, we propose that the inhibition involves a protein/protein interaction. We have previously shown that the two proteins interact in vivo and now verify by immunoprecipitation that highly purified DNA2 and FANCD2 interact in the absence of DNA. Two recent reports found that FANCD2 is purified as a dimer(Tan et al., 2020) and suggested that the dimer is not capable of DNA binding(Alcon et al., 2020; Alcon et al., 2019). It was proposed that the DNA binding defect might be due to sequestration of the DNA binding domain(Alcon et al., 2020; Alcon et al., 2019). Interestingly, FANCI did not efficiently stimulate the FANCD2-mediated inhibition of DNA2, nor did FANCI inhibit DNA2 significantly on its own. Failure to stimulate FANCD2 inhibition might be explained if the FANCD2 that inhibits DNA2 is in a dimeric form, which has also been reported to fail to interact

with FANCI(Alcon et al., 2020). The structural studies suggest that incubation of dimeric FANCD2 with FANCI leads to formation of a heterodimer that can close around DNA. Our finding suggests that this heterodimerization may not be necessary for inhibition of DNA2, though heterodimers may participate when present. We propose that free FANCD2 may directly bind to DNA2 and inhibit its nuclease activity. Otherwise, FANCD2 and/or FANCD2/FANCI heterodimer stabilize RAD51 to protect DNA from DNA2 mediated resection.

FANCD2 also interacts with several additional nucleases, such as SLX4-associated enzymes(Boisvert and Howlett, 2014) and is important for recruiting FAN1 nuclease to chromatin. FANCD2/FANCI inhibits FAN1 in vitro(Sato et al., 2016).

Links between FANCD2 and RAD51 in Fork Protection: FANCD2 Stimulates Strand Exchange by High Levels of RAD51.

We investigated and found that FANCD2, DNA2, and RAD51 coimmunoprecipitate in the presence of DNA, suggesting that RAD51 might control DNA2. RAD51 overexpression suppresses the fork protection defect of FANCD2 cells(Schlacher et al., 2012), and unstable RAD51 filaments arising due to the dominant RAD51T131P mutation in FANCR/RAD51 cases of Fanconi anemia lead to hyper-resection that can be reduced by DNA2 depletion, but not by Mre11 depletion, in vivo(Wang et al., 2015). interaction results led us to test the ability of RAD51 to inhibit DNA2. We found that RAD51 filaments indeed inhibit DNA2 biochemically. There was no inhibition in the absence of ATP. RAD51 also inhibits MRE11 at gaps behind forks, but not at fork junctions, the latter being where we propose DNA2 is primarily acting(Hashimoto et al., 2010; Kolinjivadi et al., 2017a; Kolinjivadi et al., 2017b).

We then asked what function of FANCD2 influenced RAD51. FANCD2 and BRCA2 are synthetically lethal and FANCD2 overexpression suppresses the replication fork protection defect of BRCA$^{-/-}$ cells, suggesting parallel, rather than epistatic functions(Kais et al., 2016; Michl et al., 2016). Furthermore, FANCD2/FANCI complexes stabilize RAD51 filaments (Sato). Therefore, we tested whether FANCD2 had activities similar to BRCA2 protein, a RAD51 mediator. We found that FANCD2 stimulates RAD51 strand exchange, overcoming inhibition of strand exchange by high levels of RAD51 and does so with similar stoichiometry to that reported for BRCA2(Jensen et al., 2010; Thorslund et al., 2010). BRCA2 stimulates strand exchange on one level by acting as a mediator in the exchange of RPA for RAD51 on resected overhangs. Second, BRCA2 promotes RAD51 ssDNA filament formation through inhibition of non-productive or inhibitory binding of RAD51 to dsDNA, presumably by competition between BRCA2 and RAD51 for DNA binding(Jensen et al., 2010; Thorslund et al., 2010). BRCA2 uses BRC repeats 1-4 to inhibit RAD51 ATPase and thus to stabilize filaments, but BRCA2 also uses BRC repeat 6-8 to promote nucleation of RAD51 on ssDNA and thus stimulate strand exchange(Carreira et al., 2009; Carreira and Kowalczykowski, 2011). We did not find that FANCD2 inhibited RAD51 ATPase, nor did it overcome the inhibition of RAD51 binding to

ssDNA by dsDNA (biotin pull down assays). Thus, FANCD2 is acting differently from BRCA2 or MMS22L/TONSL(Piwko et al., 2016). Furthermore, the DNA-binding-defective FANCD2-F1+F3Mut protein, was even more efficient than WT FANCD2 in enhancing strand exchange. This result suggests that stimulation of strand exchange by FANCD2 involves a significant FANCD2/RAD51 protein/protein interaction and that this in turn helps stabilize RAD51 filaments. Interestingly, the FANCD2/FANCI complex stabilizes RAD51 filaments, and FANCI DNA binding motifs are necessary but the FANCD2 DNA binding motifs are not necessary (Sato et al., 2016), in accordance with our observation that FANCD2 DNA binding mutants stimulate strand exchange even in the absence of FANCI. Stimulation of strand exchange by FANCD2 most likely involves stabilization in some way of the RAD51 filament, perhaps by preventing end release, as suggested previously for the FANCD2/FANCI complex(Sato et al., 2016) or by altering the filament structure in multiple ways, as demonstrated for RAD51 paralog(Belan et al., 2021; Berti et al., 2020; Cejka, 2021; Liu et al., 2011; Roy et al., 2021; Sullivan and Bernstein, 2018; Taylor, 1958; Taylor et al., 2015).

Given that optimum FANCD2 DNA binding is not important for stimulating strand exchange, FANCD2 might, alternatively perform a chaperone function for RAD51 filament assembly. FANCD2 has been shown to have a histone chaperone/nucleosome assembly function, and a FANCD2 mutation blocking this activity renders stalled replication forks prone to degradation(Higgs et al., 2018). Furthermore, the histone chaperone function of FANCD2 is stimulated by histone H3K4 methylation, since in BOD1L or SETD1A depleted cells, which are defective in H3K4 methylation, RAD51 filaments are destabilized and stalled forks degraded by DNA2. Thus, mutations of the FANCD2 histone chaperone activity or suppression of H3K4me correlate with destabilization of RAD51 filaments and degradation of ICL-stalled forks, largely by DNA2, albeit by a SMARCAL1/ZRANB3 independent intermediate(Higgs et al., 2018). The chaperone proposition is reasonable because many proteins with histone chaperone function, defined as promotion of nucleosome assembly, have been shown to promote other non-nucleosome protein assemblies, and FANCD2 might assist complex formation between RAD51 and DNA as well as promoting histone association and appropriate chromatin structure at stalled forks. Again, a similar function has been proposed for the RAD51 paralogs(Belan et al., 2021; Cejka, 2021; Roy et al., 2021).

There are several steps in dealing with fork stress at which stimulation of RAD51-mediated strand exchange could support fork protection and restart of stalled forks in vivo(Bhat and Cortez, 2018). First, promotion of strand exchange could stimulate RAD51 in replication fork reversal, which is BRCA2 independent(Berti et al., 2020; Mijic et al., 2017; Zellweger et al., 2015), and the reversed forks might slow replication and facilitate repair. The reversed forks might be substrates for FANCD2-regulated DNA2-mediated processing, leading to replication fork restart(Thangavel et al., 2015). Two studies did show that cells deficient in FANCD2 failed to restrain synthesis in the presence of HU or aphidicolin, possibly

by failing in fork reversal(Lossaint et al., 2013; Yeo et al., 2014). While we observed a reproducible decrease in replication fork restart and showed that DNA2 knockdown could overcome the deficit, restart was reduced but not abolished in the FANCD2 knockdown. Second, we observed that while FANCD2 inhibits resection at reversed forks, FANCD2 becomes required for repair as damage accumulates after extensive stalling with several different agents that stall or block forks (Figure 1, time courses). RAD51 (and FANCD2 when present) accumulate for repair at these late stage stalled forks(Petermann et al., 2010; Piberger et al., 2019). While it was originally thought that the structure of the forks at these extensively damaged chromosomes might be DSBs, recent evidence suggests that they may also be unrepaired gaps after repriming, by Prim-Pol, at leading strand blocks or by pol α–primase at blocks on the lagging strand, especially(Quinet et al., 2019). FANCD2 might stimulate RAD51-mediated post-replication repair and template switch at these sites, especially if BRCA2 is defective(Fumasoni et al., 2015). A completely different possibility, aside from protection of stalled replication forks, is that the strand exchange stimulation function of FANCD2 may be its important contribution to the late stages of ICL repair by the FA pathway, which involves repair of DSBs(Duxin and Walter, 2015).

To recapitulate, our model (Figure 7) taking cumulative data to date into account, suggests that DNA2 is required for resection of transiently stalled reversed forks to promote restoration of active forks without collapse to DSBs or gaps. FANCD2 is required to keep DNA2/MRE11 mediated resection in a range consistent with preserving genome stability and restoring forks, as demonstrated previously by increased chromosomal aberrations in its absence(Schlacher et al., 2012). FANCD2 does so by inhibiting DNA2 and perhaps MRE11. However, even if FANCD2 is present, extensive or prolonged stalling, or strong fork blocking lesions, such as CPT or cisplatin, lead to the emergence of genome destabilizing structures that require an additional repair mechanism(s) involving resection. FANCD2 then becomes essential for resection. This observation at stalled forks is reminiscent of events at forks stalled by 24 h ICL inhibition, where FANCD2 recruits CtIP, which augments resection by DNA2/BLM, channeling repair of obligate DSB intermediates in the ICL repair pathway into HR instead of toxic NHEJ and or recruits pol theta. In addition to promoting resection, our study suggests that FANCD2 may further stimulate strand exchange required for repair. In BRCA2$^{-/-}$ cells excessive resection creates a substrate that requires MUS81 for restart(Lemacon et al., 2017). The MUS81-cleaved intermediate, a one-ended DSB, may then be repaired by recombination dependent mechanisms such as template switch post-replication repair, which requires RAD51, and/or break-induced replication, which requires pol δ, or translesion synthesis. The stimulation of RAD51 by FANCD2 in strand exchange that we observe could be necessary for such fail-safe mechanisms of completing replication (Figure 6). Yet another repair mechanism at stressed replication forks is dependent on post-replication repair of gaps introduced by repriming downstream of lesions instead of DSBs and could also compensate for or substitute

for over-resected reversed forks. In the presence of FANCD2 we see increasing phospho-RPA during stalling which implies activation of ATR, which is presumably necessary for repair. ATR has been shown by fiber tracking to activate Prim-Pol and repriming and to promote gaps in nascent DNA (Quinet and Vindigni, 2019). In FANCD2-depleted cells, this pathway cannot be activated effectively because RPA-p does not accumulate, blunting the checkpoint and recovery and leading to genome instability. FANCD2 has also been reported to counteract NHEJ at IR-induced DSBs, and FANCD2 deficient cells show increased toxic NHEJ, decreased resection, and decreased recombinational repair(Cai et al., 2020). FANCD2 has also been implicated in counteracting Ku70 inhibition of repair(Pace et al., 2010). RAD51 strand exchange stimulation might also explain the minor defect in DSB repair pathways in the absence of FANCD2 reported previously(Nakanishi et al., 2011). The role of FANCD2 in fork protection may be compensated for by either BRCA2, for HR-like fork protection, or in a by-pass mechanism by pol theta/CtIP recruitment for alt-EJ(Kais et al., 2016).

The Importance of Regulating DNA2 Nuclease Activity

Inhibition by FANCD2 represents a new aspect of the regulation of DNA2, which has already been shown to be modulated by multiple other mechanisms [see(Zheng et al., 2020) for recent review]. It is interesting that in FANCD2 cells inhibition of either MRE11 nuclease or DNA2 nuclease protects forks from degradation after mild HU treatment. We and others have found that DNA2 and MRE11 have a similar, possibly “epistatic” relationship in fork protection in BRCA$^{-/-}$ cells(Liu et al., 2016; Ray Chaudhuri et al., 2016). Therefore, it is interesting that MRE11, like DNA2, is inhibited by FANCD2 in vitro in our studies (Figure 3G). Nevertheless, the absence of FANCD2 inhibition of EXO1 (Figure 3H) shows that there is specificity in the regulation of nucleases by FANCD2.

We note that we previously showed that DNA2 inhibitors synergize with PARPi (PARP inhibitors) in killing MCF7 breast cancer cells(Liu et al., 2016). PARP has been implicated in protection of stalled forks from unligated Okazaki fragments such as occur in FEN1 or LIG1 deficiency(Hanzlikova et al., 2018) and in protection from DNA2-dependent degradation of nascent DNA, which is proposed to occur on the lagging strand(Thakar et al., 2019). We may be observing over-resection on the lagging strand in FANCD2$^{-/-}$ cells at early times of fork stalling that leads to reversed forks in our studies. PARPi causes fork speed acceleration and enhanced replication fork speed can in itself cause genome instability and may involve unligated Okazaki fragments(Maya-Mendoza et al., 2018; Merchut-Maya et al., 2019). Knockdown of FANCD2 leads to increased fork speed upon prolonged replication stress conditions(Lossaint et al., 2013; Yeo et al., 2014). Lagging strand events are another type of damage that must be considered in interpreting our results.

Synthetic Viability and Fanconi Anemia

This study began as a discovery of synthetic viability between DNA2 and FANCD2 defects. We and others have shown that additional FANC alleles show over-resection that is reduced by depletion of DNA2, suggesting that additional proteins are required to fully reconstitute FANCD2-regulated resection at stalled forks (Rickman et al., 2020). Interestingly, different mechanisms of fork protection are seen with different types of damage(Rickman et al., 2020) and with different fork protection factors(Liu et al., 2020). Many additional genes show synthetic viability with FA complementation groups FA-A, FA-C, FA-I, FA-D2, FA, such as BLM helicase(Velimezi et al., 2018). One of the major functions of BLM is to complex with DNA2 in double-strand end resection(Cejka et al., 2010; Nimonkar et al., 2011). BLM is also deleterious for fork protection and replication fork restart in FANCD2 deficient cells, and depletion of BLM rescues restart in that case(Schlacher et al., 2012). It is possible that BLM is also required at reversed forks to promote degradation by DNA2 (and/or EXO1, which is stimulated BLM). These results have significant impact on our goal of using inhibition of DNA2 to increase the therapeutic index for treating Fanconi anemia patients with various cancers by protecting normal, non-cancerous cells from cisplatin.

Acknowledgments

This work was supported by a CIHR foundation grant (J.-Y.M.) and J.-Y.M. is a FRQS Chair in genome stability; Korean government grants NRF-2017R1A2B2002289 and RF-2018R1A6A1A0302514 for W.C. sabbatical funding; R50CA211397 to L.Z.; R011CA085344 to B.S.; and USPS grant GM123554 to JLC.

Author Contributions

Conceptualization, J.C.; Methodology, W.L., I.R., P.P., Y.M., M.C., Y.X., C.L., Q.W., L.Z.; Writing – Original Draft, W.L., P.P., J.C.; Writing – Review and Editing, W.L., L.Z., J.M., B.S, J.C.; Funding Acquisition, W.C., J.M., B.S., J.C; Supervision J.M., B.S., J.C.

Competing Interests

The authors declare no competing interests.

Key Resources Table

REAGENT or RESOURCE	SOURCE	IDENTIFIER
Antibodies		
Mouse monoclonal anti-MUS81	Abcam	ab14387
Rabbit polyclonal anti-SMARCAL1	Bansbach et al., 2009	
Rabbit polyclonal anti-ZRANB3	Bethyl	A303-033A
Mouse monoclonal anti-GAPDH	Millipore	MAB374
Mouse monoclonal anti-BrdU (IdU)	BD Biosciences	347580
Rat monoclonal anti-BrdU (CldU)	Abcam	ab6326
Mouse monoclonal anti-BrdU for IF	Abcam	ab8152
Goat anti-rat Alexa Fluor 594	Thermo Fisher	A-11007
Goat anti-mouse Alexa Fluor 488	Thermo Fisher	A-11029
Rabbit polyclonal anti-DNA2	Abcam	ab96488
Mouse monoclonal anti-MRE11	GeneTex	GTX70212
Mouse monoclonal anti-FANCD2	Santa Cruz biotechnology	sc-20022
Rabbit polyclonal anti-SLX4	Bethyl	A302-269A-1
Rabbit polyclonal anti-RAD51	Abcam	ab133534
Phospho-Histone H2A.X (Ser139)	Cell Signaling Technology	#2577
Mouse monoclonal anti-GAPDH	Millipore	AB2302
RPA2 S33 phosphorylation	Abcam	ab211877
RPA2 T21 phosphorylation	Abcam	ab109394
Mouse monoclonal anti-FLAG	Sigma	F1804
Mouse monoclonal anti-RPA2	Abcam	Ab2175
Mouse monoclonal anti-His tag	Proteintech	66005-1
Rabbit polyclonal to Histone H3	Abcam	Ab1791
Chemicals and reagents		
Hydroxyurea	Sigma-Aldrich	H8627
Camptothecin	Sigma-Aldrich	PHL89593
MRE11 protein	Tanya Paull, UT Austin	
EXO1 protein	Paul Modrich, Duke University	
RuvC	Abcam	ab63828
Recombinant human RAD51	Abcam	ab81943
Cisplatin	Sigma-Aldrich	1134357
Protease inhibitor cocktail	Roche	05892970001
Genmute	SignaGen	SL100568
CldU	Sigma-Aldrich	C6891-100MG

IdU	Sigma-Aldrich	I7125-5G
Critical Commercial Assays		
Neutral COMET assay	Trevigen	
Combing assay kit	Genomic Vision	
Cell Lines		
Cell line	Source	
U2OS	ATCC	
HEK293T	ATCC	
A549	ATCC	
BL21(DE3) CodonPlus	Agilent Technologies	Cat#230280
PD352i	FA Cell Repository at the Oregon Health & Science University	
Plasmids		
pLKO.1 shSCR	Karanja et al., 2012	
pLKO.1 shDNA2	Karanja et al., 2012	
pCMVΔR8.2	Karanja et al., 2012	
pCMV-VSV-G	Karanja et al., 2012	
pET15b-FANCD2-His	Takahashi et al., 2014	
pCMV7.1-FLAG-DNA2	Lin et al., 2013	
siRNA sequence		
Gene name	Sequence	
SMARCAL1	GCUUUGACCUUCUUAGCAA	
ZRANB3	GAUUCGAUCUAAUAACAGU	
SLX4#2	GAAGUGGAAUUGUCUAGCA	
FANCD2 pool of 4	UACCUCAAGUGUAUCCAUG	
	GGAGAUUGAUGGUCUACUA	
	CAACAUACCUCGACUCAUU	
	GGAUUUACCUGUGAUAAUA	
BRCA2	GAAACGGACUUGCUAUUUA	
MRE11	GCUAAUGACUCUGAUGAUATT	
CTIP	GCUAAAACAGGAACGAAUCTT	
RAD51#1	CGAUGUGAAGAAAUUGGAATT	
RAD51 J12	Bhat et al., 2018	
DNA2	ACAGUUGCCUGCAUUCUAA	
FANCM	AGACAUCGCUGAAUUUAAA	
MUS81	CAUUAAGUGUGGGCGUCUA	
Oligonucleotide substrates		

Name	Sequence
JYM945	ACGGCATAAAGCTTGACGATTACATTGCTAGGACATCTTTGCCCACCTGCAG-GTTCACCC (Shibata et al., 2014)
87 FORK	TTCACGAGATTTACTTATTTCACTGCGGCTACATGATGCATCGTTAGGCGATT-CCGCCTAACGATGCATCATGTTGTTACCCTTTGA
LU 5' FLAP	TTCACGAGATTTACTTATTTCACTGCGGCTACATGATGCATCGTTAGGCGATT-CCGCCTAACGATGCATCATGTCGCGAACCCTATTTAGGGTTCGCG
LU 3' FLAP	CGCGAACCCTATTTAGGGTTCGCGACATGATGCATCGTTAGGCGATTCCGCC-TAACGATGCATCATGTTTCACGAGATTTACTTATTTCACTGCGGCT
Strand 1	CGCTGCCGAATTCTACCAGTGCCATTGCTTTGCCCACCTGCAGGTTCACC
Strand 2	GGTGAACCTGCAGGTGGGCAAAGCAATAGTAATCGTCAAGCTTTATGCCG
Strand 3	CGGCATAAAGCTTGACGATTACTATTGGCTGTCTAGAGGATCCGACTATC
Strand 4	GATAGTCGGATCCTCTAGACAGCCAATGGCACTGGTAGAATTCGGCAGCG
Strand 1L	TTCACGAGATTTACTTATTTCACTGCGGCTCGCTGCCGAATTCTACCAGTGC-CATTGCTTTGCCCACCTGCAGGTTCACC
JYM925	GGGTGAACCTGCAGGTGGGCAAAGATGTCCTAGCAATGTAATCGTCAAGCTT-TATGCCGT (Shibata et al., 2014)
EXO1: 3' overhang	ACATGATGCATCGTTAGGCGATTCCGCCTAACGATGCATCATGTTTCACGAG-ATTTACTTATTTCACTGCGGCT
EXTJYM925	CCTATGATCATTCCTTAAGGCTATCCTGAGTACCTCAGTCGGGTGAACCTGC-AGGTGGGCAAAGATGTCCTAGCAATGTAATCGTCAAGCTTTATGCCGT
RJ-167	CTGCTTTATCAAGATAATTTTTCGACTCATCAGAAATATCCGTTTCCTATATTTATTCCTATTATGTTTTATTCATTTACTTATTCTTTATGTTCATTTTTTATATCCTTTACTTTATTTTCTCTGTTTATTCATTTACTTATTTTGTATTATCCTTATCTTATTTA (Jensen et al., 2010)
RJ-PHIX-42-1	CGGATATTTCTGATGAGTCGAAAAATTATCTTGATAAAGCAG (Jensen et al., 2010)
RJ-PHIX-42-2	TAATACAAAATAAGTAAATGAATAAACAGAGAAAATAAAGGC

RJ-Oligo1	TAATACAAAATAAGTAAATGAATAAACAGAGAAAATAAAG (Jensen et al., 2010)
RJ-Oligo2	CTTTATTTTCTCTGTTTATTCATTTACTTATTTTGTATTA (Jensen et al., 2010)
RJ-Oligo3	AATTTTTCGACTCATCAGAAATATCCGTTTCCTATATTTA
RJ-Oligo4	TAAATATAGGAAACGGATATTTCTGATGAGTCGAAAAATT
3'Bio-RJ-PHIX-42-1	CGGATATTTCTGATGAGTCGAAAAATTATCTTGATAAAGCAG/3Bio/ (Jensen et al., 2010)
Oligo#90	CGGGTGTCGGGGCTGGCTTAACTATGCGGCATCAGAGCAGATTGTACTGAGAGTGCACCATATGCGGTGTGAAATACCGCACAGATGCGT (Jensen et al., 2010)
Oligo#60	ACGCATCTGTGCGGTATTTCACACCGCATATGGTGCACTCTCAGTACAATCTGCTCTGATGCCGCATAGTTAAGCCAGCCCCGACACCCG (Jensen et al., 2010)

Lead Contact and Materials Availability

Further information and requests for resources and reagents should be directed to and will be fulfilled by the Lead Contact, Judith L. Campbell (jcampbel@caltech.edu). All unique/stable reagents generated in this study are available from the Lead Contact without restriction.

Method Details

Cell Culture and Cytotoxicity Assays

U2OS, A549, PD352i and PD20 and PD20 with FANCD2 complemented cells were cultured in DMEM medium with 10% FBS. Survival fraction data of PD352i for cisplatin treatment was determined by cytotoxicity assay according to a protocol described previously (Karanja et al., 2012). Briefly, after puromycin selection, $5x10^4$ cells were plated in a 24 well plate, followed by cisplatin treatment for 3 days; cells were fixed and stained with 1% crystal violet in methanol; and viability count determined by imaging cell density using near infrared imaging (Li-Cor).

Lentivirus Production and DNA2 Knockdown

Lentivirus production and DNA2 shRNA sequence were as previously described (Karanja et al., 2012). Briefly, cells were co-transfected with pLKO.1 shSCR or pLKO.1 shDNA2 and

pCMVΔR8.2 and pCMV-VSV-G plasmids. Fresh complete medium was changed every 24 hours post-transfection. Virus were harvested with filtration at 48 hours and 72 hours post-transfection. The infection was performed on A549 cells and PD352i cells with overnight incubation, followed by puromycin selection for two days.

Nuclear Fractionation

Cells ($1x10^6$) were harvested and washed with PBS, then lysed on ice for 20 min with 100 μl H150 buffer, which contains 50 mM HEPES (pH7.4), 150 mM NaCl, 10% glycerol, 0.5% NP-40 and protease inhibitor cocktail (Roche). The lysate was spun for 10 min at 5000g, and the supernatant is the cytoplasmic fraction. The pellet was washed two times with H150 lysis buffer, and the supernatant discarded. The pellet is the nuclear fraction. The pellet was resuspended in PBS (20 μl) and 20 μl 2xSDS loading buffer and boiled for western blot.

Immunofluorescence for native BrdU staining and EdU staining

BrdU staining was carried out as described (Couch et al., 2013). Briefly, cells ($1x10^5$ labeled with BrdU and EdU as described in the legend to Figure 1 were plated on coverslips, washed with PBS, pre-extracted with ice cold 0.5% Triton-X100 for 4 min, then fixed with 4% paraformaldehyde for 10 min, permeabilized with 0.1% Triton-X100 for 2 min and then washed with PBS 3 times. Blocking was carried out with 1% BSA in PBS for 1 h. For EdU detection, a 1 ml click reaction containing 5 μl 1 mM Azide-488 (Invitrogen), 100 μl 20 mg/ml sodium ascorbate, 20ul 100mM $CuSO_4$) was performed to detect incorporated EdU. Then FANCD2 antibody 1:200 in blocking buffer incubated overnight at 4 degree. For BrdU staining, slides were incubated with BrdU and FANCD2 primary antibody overnight at 4°C. The slides were washed in PBS three times and then incubated with secondary antibody (1:200, Alexa Fluor 594 and 488 from Invitrogen) for 1 h at room temperature. The slides were washed with PBS 3 times and mounted with Prolong Gold AntiFade Reagent with DAPI (Invitrogen P36941).

Plasmid and siRNA Transfection

A549 and U2OS cells were plated the day before transfection. 20 nM siRNA was used for single and 16 nM for each siRNA in co-transfection. Cells was transfected with Genmute and labeled as indicated 72 hours post-transfection. DNA2 plasmid transfection was described previously (Liu et al., 2016).

DNA Fiber Assay

DNA fiber spreading and staining were performed as previously described (Liu et al., 2016). Briefly, 1000 labeled cells (2 μl, 500 cells per μl) on slides were half dried, 10 μl lysis buffer (0.5% SDS, 200 mM Tris-HCl pH 7.4, 50 mM EDTA) was added, followed by incubation for 6 min at room temperature. The slide was tilted to 15 degrees to allow the DNA to run slowly

down the slide. Slides were air dried for at least 40 minutes, and fixed for 2 min in 3:1 methanol: acetic acid in a coplin jar. Slides were dried in a hood for 20 min. Slides were treated with 2.5 M HCl for 70 min for denaturation and then washed with PBS 3 times and blocked with 10% goat serum in PBST (0.1% Triton-X100 in PBS) for 1 h. Slides were incubated with the rat anti-BrdU and mouse anti-BrdU antibody, 1:100, for 2 h, washed 3 times with PBS, and then incubated with secondary antibody (Goat anti-Mouse 488 and Goat anti-Rat 594, Invitrogen) at 1:200. Slides were imaged with immunofluorescence microscopy and fiber length measured by Nikon software. Statistical analyses were completed using Prism. An ANOVA test was used when comparing more than two groups followed by a Dunnett multiple comparison post-test.

Neutral COMET assay

The neutral COMET assays were performed in accordance with the manufacturer's (Trevigen) instructions. Cells were trypsinized and washed, then palleted, resuspended with low melt agarose, then dropped on the slides. After cool down, the slides were incubated in cold lysis buffer (Trevigen) for 1 hour, then incubated in running buffer for 30 minutes, and then subjected to electrophoresis at 21 volts for 45 minutes. Slides were then immersed in precipitation buffer (Trevigen) and 70% ethanol for 30 minutes, respectively. Slides were dried overnight and stained with SYBR green I (Thermofisher). Slides were imaged with fluorescence microscope with FITC channel.

DNA Combing Assay

The assay was performed with the Molecular Combing Kit from Genomic Vision. Briefly, after indicated labeling treatment, U2OS cells ($2x10^5$ cells) in 40μl cold PBS were harvested and plugs prepared with Buffer 2 according to the manufacturer's instructions. Plugs were immersed in Buffer 3 (added component 3), and incubated at 50°C in a water bath overnight. Plugs were washed 3 times with DNase free TE buffer and then treated with Agarase overnight at 42°C in MES buffer. The suspension was diluted with Buffer 4 and the DNA combed on the cover slip (Genomic Vision) with the DNA combing instrument (Genomic Vision). The cover slip was baked at 65°C for 2 h, DNA was denatured by incubating the coverslip with 0.5 M NaOH and 1 M NaCl for 8 min at room temperature, washed with PBS and blocked with 10% goat serum in PBS and 0.1% Triton. The cover slip was incubated with 1:25 rat anti-BrdU (ab6326 Abcam) and 1:5 mouse anti-BrdU (BD B44) primary antibody for 1 h, washed with PBS, and incubated with secondary antibody (Thermo, Goat anti Rat 594 and Goat anti Mouse 488). The cover slip was mounted and imaged with an immunofluorescence microscope. The fiber length was measured by Nikon software. Statistical analyses were completed using Prism. An ANOVA test was used when comparing more than two groups followed by a Dunnett multiple comparison post-test.

Immunoprecipitation

For FLAG pulldown assays and immunoprecipitation assays, 293T cells were transfected with or without RAD51 vector (or FLAG-DNA2 vector) using the Polyjet (SignaGen SL100688) transfection reagent. 24 h after transfection, the cells were incubated with or without 2 mM HU for 3 h. Cells ($1x10^7$) were collected and lysed by brief sonication and incubation in the immunoprecipitation (IP) buffer H150 (50 mM HEPES-KOH (pH7.4), 150 mM NaCl, 0.1% NP40 and 10% glycerol) with protein inhibitor cocktail (Thermo Fisher) for 30 min. After centrifugation (20,000g, 15 min, 4°C), the supernatants were collected and the protein concentration determined. Cell lysate (1 mg) was pre-cleaned with 10 μl Protein A/G beads (Thermo #88802) for 1 h. After removing beads, the lysate was incubated with 2 μg (1μg/μl) anti-RAD51 (ab133534 Abcam) or anti-FLAG M2 magnetic beads for FLAG pulldown (Sigma). Then 10 μl Protein A/G magnetic beads were added and incubated overnight at 4°C. The beads were washed three times with the IP buffer H150 and boiled in 1x SDS-PAGE loading buffer directly. The DNA2 and FANCD2 were analyzed by western blot analysis.

Oligonucleotides

Oligonucleotide substrates for enzymatic assays were labeled at the 5' end with ^{32}P using polynucleotide kinase. The sequences are listed in the Key Resources Table. For DNA2 assays, single-stranded DNA was JYM945 (Shibata et al., 2014). The forked substrate was designated 87 FORK. The 5' flap substrate was LU 5' FLAP. The 3' flap substrate was LU 3'. The reversed fork with blunt ends consisted of 4 oligonucleotides: strand 1, strand 2, strand 3 and strand 4 in the Key Resources Table (van Gool et al., 1998). The reversed fork with 5' overhang consisted of strand1L, strandFANCD2, strand3, and strand4.

The MRE11 nuclease duplex substrate was formed by annealing 5' labeled JYM945 to JYM925 (Shibata et al., 2014). This was also used for binding of RAD51 to dsDNA. For the EXO1 assay, a hairpin with a 3' overhang was used.

For RAD51 binding, JYM945 was used. For RAD51 strand exchange assays the single-stranded DNA was EXTJYM925: The 60mer duplex was formed by annealing labeled JM945 to JM925 (see MRE11 substrate).

Proteins

Recombinant human RAD51 was from Abcam (ab81943) and tested for ATPase, strand exchange, and DNA binding. RuvC was Abcam (ab63828). MRE11 was the gift of Tanya Paull (UT Austin) and EXO1 (0.77 mg/ml) was a gift from Paul Modrich, Duke University. Sources of FANCD2 and DNA2 are described in the text or figure legend describing the experiments in which they were used.

FANCD2-His Purification from *E. coli*

Human FANCD2 protein was purified from *E. coli* as previously described (Takahashi et al., 2014). The FANCD2 vector was transformed into BL21(DE3) CodonPlus (Agilent Technologies 230280) cells. 20 L of transformed cells were amplified at 30°C, 250 rpm. FANCD2 protein was produced by adding 0.5 mM IPTG at 16°C for 18 hours, when the cell density reached an OD_{600}=0.6. The *E. coli* cells were harvested and pelleted and lysed in Buffer A (50 mM Tris-HCl PH8.0, 500 mM NaCl, 5 mM 2-mercaptoethanol, 1 mM phenylmethylsulfonyl fluoride (PMSF), 12 mM imidazole, and 10% glycerol), and disrupted by sonication. The lysate was centrifuged at 20,000 g at 4°C; the supernatant was mixed gently by the batch method with 3ml of Ni-NTA agarose beads, at 4°C for 1h. The beads were packed into an Econo-column, and were washed with 67 column volumes of buffer A. The His-tagged FANCD2 were eluted with a 20 column volumes linear gradient of 12-400 mM imidazole in buffer A. The peak fractions were collected. To remove His tag from the FANCD2 protein, thrombin protease (2U/mg GE healthcare) was added, and the sample was then dialyzed against 4L of buffer B (20 mM Tris-HCl, pH8.0, 200 mM NaCl, 5 mM 2-mercaptoethanol, 10% glycerol). Afterward, the sample was passed through a Q Sepharose Fast Flow (2.5 ml, GE Healthcare) column. The resin was washed with 60 column volumes of buffer B containing 250 mM NaCl. Human FANCD2 was then eluted with a 20 column volume linear-gradient of 250 mM-450 mM NaCl in buffer B. The peak fractions were collected, and human FANCD2 was further purified by gel filtration chromatography on a Superdex 200 column (GE Healthcare) equilibrated with Buffer B containing 200 mM NaCl. The purified FANCD2 was concentrated, frozen in aliquots, and stored at -80°C. The concentration of purified FANCD2 was determined by the Bradford method, using BSA as standard.

FLAG-DNA2 Purification from Mammalian ells

The FLAG-DNA2 expression and purification procedure was as described previously (Lin et al., 2013). In brief, whole cell lysates were incubated with the M2 FLAG magnetic beads (Sigma) for at least 6 h in cold room. After extensively washing with a buffer containing 50 mM Tris-Cl (pH 7.5) and 500 mM NaCl, the bound proteins were eluted with 3X FLAG peptide (Sigma). The purity of DNA2 proteins was analyzed by 4–15% gradient SDS–polyacrylamide electrophoresis (SDS–PAGE) and Coomassie brilliant blue staining, and the concentration was determined by comparison to BSA after Coomassie blue staining of SDS gels.

Mapping the FANCD2 binding domain in DNA2

Mutant FLAG-DNA2 proteins were prepared using site-directed mutagenesis. The N-terminal deletions were made using the HiFi DNA cloning kit from NEB to excise portions of the N-terminus of the gene, while C-terminal deletions were made by the insertion of a stop codon earlier in the gene construct. Coimmunoprecipitations were performed by overexpressing the

DNA2 proteins in HEK-293T cells prior to making cell lysates. FANCD2 was added to the lysates to a final concentration of 2 nM protein to ensure measurable interaction with DNA2. The FANCD2:DNA2 complex was pulled down using a FANCD2 antibody attached to magnetic beads. The beads were washed prior to eluting the samples using SDS loading buffer, and the samples were analyzed by western blot using a 3XFLAG antibody.

Strand Exchange Assays

Single-stranded DNA (EXTJYM925) was preincubated in the presence of RAD51 and FANCD2 in a reaction mixture containing 25 mM TrisOAc (pH 7.5), 2 mM MgCl2, 2 mM CaCl2, 2 mM ATP, 1 mM DTT and 0.1 mg/ml BSA for 5 min at 37˚C for filament formation. Following pre-incubation, dsDNA (5' labeled JYM945 annealed to JYM925) with the labeled strand complementary to the filament, was added to the reaction mixture and incubation was continued for an additional 30 min at 37˚C for strand exchange. Reactions were terminated by the addition of proteinase K and SDS to 0.5 mg/ml and 0.25% respectively and incubated for 10 min at 37°C. 1 µL of Loading Buffer (2.5% Ficoll-400, 10 mM Tris-HCl, pH 7.5, and 0.0025% xylene cyanol) was added and samples were loaded on an 8% native gel using 29:1 30% acrylamide solution. Gels were run at 100v (constant voltage) for 4 h.

For strand exchange assays that used the 3' overhang DNA (RJ-167 annealed to RJ-PHIX-42-1) for filament formation during preincubation, 5' labeled dsDNA (5' labeled RJ-Oligo1 annealed to RJ-Oligo2) was used as its respective strand exchange target during the 30 min incubation. Similarly, in instances using 5' overhang DNA (RJ-167 annealed to RJ-PHIX-42-2) to generate filaments, 5' labeled dsDNA (5' labeled RJ-Oligo4 annealed to RJ-Oligo3) was used as its double-stranded target.

Biotin Pull-down assays for RAD51 and FANCD2 association with overhang DNA.

The protocol was adopted from Jensen et al., 2010. Briefly, the oligonucleotide substrate Bio-RJ-PHIX-42-1 composed of the same sequence as RJ-PHIX-42-1 but containing a 3′ biotin modification was obtained from IDT (Integrated DNA Technologies) and PAGE purified. The biotinylated 3' overhang substrate was generated by annealing Bio-RJ-PHIX-42-1 to oligonucleotide RJ-167 at a 1:1 molar ratio in STE buffer. Competitor heterologous dsDNA was similarly generated by annealing PAGE purified oligonucleotides Oligo#90 and Oligo#60. For pull-down, RAD51 and FANCD2 proteins were incubated in Buffer S (25 mM TrisOAC pH 7.5, 1 mM MgCl2, 2 mM ATP, 1 mM DTT, and 0.1 µg/µL BSA) for 15 min at 37˚C followed by the addition of 3' overhang DNA (162 nt RJ-167 annealed to 42 nt 3' Bio-RJ-PHIX-42-1) and competitor heterologous dsDNA (90mer, Oligo #90/Oligo #60 oligonucleotides) and the reaction was incubated for an additional 5 min at 37˚C. Where DNA was omitted, TE buffer was used and similarly, respective proteins storage buffers were used where proteins were

omitted. DNA-protein complexes were captured by adding the reaction mixtures to 2.5 µL of MagnaLink Streptavidin magnetic beads (Solulink) pre-washed by excess Buffer S supplemented with 0.1% Ipegal CA-630 and rotating for 10 min at 25˚C. Bead complexes were then washed with excess Buffer S supplemented with 0.1% Ipegal CA-630. Protein was then eluted by re-suspending in 15 µL of 2X protein sample buffer and heating at 54˚C for 4 min. The elution fraction was then loaded into a Bis-Tris protein gel for western analysis. Following transfer, the membrane was cut horizontally at the 70 kD marker to separately probe for RAD51 and FANCD2. The lower half was probed using 1:1000 diluted α-RAD51 (Abcam) and the upper half using 1:1000 diluted α-FLAG (ThermoFisher) to detect FANCD2. Anti-mouse (LI-COR) secondary antibody diluted 1:10,000 was used and membranes were imaged via Odyssey imaging system. Bands were quantified using ImageQuant (Cytiva) software.

Nuclease and DNA-dependent ATPase Assays

DNA2 nuclease assay: FANCD2-His or FANCD2-His diluent was incubated in DNA2 nuclease reaction mix (50 mM HEPES-KOH, pH 7.5, 5 mM $MgCl_2$, 2mM DTT, 0.25 mg/ml BSA) for 30 min at 4°C. DNA2, preincubated with substrate (87 fork, 1.5 nM molecules) for 5 min on ice, was added and the reaction was incubated for 30 min at 37°C. See Key Resources Table for substrate sequences. Following incubation, proteinase K and SDS were added to 1 mg/ml and 0.5%, respectively, and incubation continued for 10 min at 37°C. Denaturing termination dye (2X: 95% deionized formamide, 10 mM EDTA, 0.1% bromophenol blue and 0.1% xylene cyanol) was added and the mixture boiled for 5 min. Samples were run on a sequencing gel and the gel analyzed by phosphor imaging.

MRE11 nuclease assay: MRE11 reaction mixtures contained 25 mM MOPS (pH 7.0), 60 mM KCl, 0.2% Tween 20, 2 mM DTT, and 1 mM $MnCl_2$ as described (Paull and Gellert, 1998). MRE11 and blunt dsDNA 60mer substrate (JYM925/JYM945 oligonucleotides) were incubated together on ice for 5 min before being introduced to the reaction mixture at 200 nM and 1 nM, respectively, and incubated for 30 min at 37°C. Following incubation, reactions were terminated by adding proteinase K and SDS was added to 1 mg/ml and 0.5% respectively and incubated for 10 min at 37°C. 10 µl of 2X termination dye was added and samples boiled for 5 min. After denaturing, samples were run on a 12% sequencing gel at constant 60W and the gel analyzed by phosphor imaging.

EXO1 nuclease assay: Conditions are as previously described (Shao et al., 2014). Reaction mixtures (10 µl) contained 20 mM Tris-HCl, pH 7.6, 0.75 mM HEPES-KOH, 120 mM KCl, 250 µg/ml BSA, 2 mM ATP, 1 mM glutathione, 2 mM $MgCl_2$, 1% glycerol, 0.06 mM DTT, 1.5 nM substrate and EXO1 (0.77 nM).

ATPase assays. The DNA-dependent ATPase assays were carried out as previously described (Masuda-Sasa et al., 2006). Reaction mixtures (10 µL) contained 20 mM TrisOAc

(pH 7.5), 4 mM $MgCl_2$, 4 mM $CaCl_2$ (where shown), 1 mM DTT, 0.5 mM ATP, 20 μCi/ml [γ-32P]-ATP, and 900 nM (in nucleotides) of cold ssDNA (60 nt, oligonucleotide JYM945). Indicated concentrations of FANCD2 and 300 nM RAD51 were incubated in reaction mixture for 90 min at 37˚C and then reactions were stopped by the addition of EDTA to 4 mM. All reactions contained equal amounts of FANCD2 diluent.

Quantification and Statistical Analysis.

Statistical analyses were completed using Prism. An ANOVA test was used when comparing more than two groups followed by a Dunnett multiple comparison post-test. A two-tailed t-test was used to compare two samples with normally distributed data. No statistical methods or criteria were used to estimate sample size or to include/exclude samples.

Data and Code Availability

REFERENCES

Alcon, P., Shakeel, S., Chen, Z.A., Rappsilber, J., Patel, K.J., and Passmore, L.A. (2020). FANCD2-FANCI is a clamp stabilized on DNA by monoubiquitination of FANCD2 during DNA repair. Nat Struct Mol Biol *27*, 240-248.

Alcon, P., Shakeel, s., Patel, K.J., and Passmore, L.A. (2019). FANCD2-FANCI is a clamp stabilized on DNA by monoubiquitination during DNA repair BioRxiv.

Badie, S., Carlos, A.R., Folio, C., Okamoto, K., Bouwman, P., Jonkers, J., and Tarsounas, M. (2015). BRCA1 and CtIP promote alternative non-homologous end-joining at uncapped telomeres. EMBO J *34*, 828.

Belan, O., Barroso, C., Kaczmarczyk, A., Anand, R., Federico, S., O'Reilly, N., Newton, M.D., Maeots, E., Enchev, R.I., Martinez-Perez, E.*, et al.* (2021). Single-molecule analysis reveals cooperative stimulation of Rad51 filament nucleation and growth by mediator proteins. Mol Cell *81*, 1058-1073 e1057.

Berti, M., Ray Chaudhuri, A., Thangavel, S., Gomathinayagam, S., Kenig, S., Vujanovic, M., Odreman, F., Glatter, T., Graziano, S., Mendoza-Maldonado, R.*, et al.* (2013). Human RECQ1 promotes restart of replication forks reversed by DNA topoisomerase I inhibition. Nat Struct Mol Biol *20*, 347-354.

Berti, M., Teloni, F., Mijic, S., Ursich, S., Fuchs, J., Palumbieri, M.D., Krietsch, J., Schmid, J.A., Garcin, E.B., Gon, S.*, et al.* (2020). Sequential role of RAD51 paralog complexes in replication fork remodeling and restart. Nat Commun *11*, 3531.

Betous, R., Couch, F.B., Mason, A.C., Eichman, B.F., Manosas, M., and Cortez, D. (2013). Substrate-selective repair and restart of replication forks by DNA translocases. Cell Rep *3*, 1958-1969.

Bhat, K.P., Betous, R., and Cortez, D. (2015). High-affinity DNA-binding domains of replication protein A (RPA) direct SMARCAL1-dependent replication fork remodeling. J Biol Chem *290*, 4110-4117.

Bhat, K.P., and Cortez, D. (2018). RPA and RAD51: fork reversal, fork protection, and genome stability. Nat Struct Mol Biol *25*, 446-453.

Bhat, K.P., Krishnamoorthy, A., Dungrawala, H., Garcin, E.B., Modesti, M., and Cortez, D. (2018). RADX Modulates RAD51 Activity to Control Replication Fork Protection. Cell Rep *24*, 538-545.

Boisvert, R.A., and Howlett, N.G. (2014). The Fanconi anemia ID2 complex: dueling saxes at the crossroads. Cell Cycle *13*, 2999-3015.

Budd, M.E., and Campbell, J.L. (2000). The pattern of sensitivity of yeast dna2 mutants to DNA damaging agents suggests a role in DSB and postreplication repair pathways. Mutat. Res. *459*, 173-186.

Budd, M.E., Reis, C.C., Smith, S., Myung, K., and Campbell, J.L. (2006). Evidence suggesting

that Pif1 helicase functions in DNA replication with the Dna2 helicase/nuclease and DNA polymerase delta. Mol Cell Biol *26*, 2490-2500.
Bugreev, D.V., and Mazin, A.V. (2004). Ca2+ activates human homologous recombination protein Rad51 by modulating its ATPase activity. Proc Natl Acad Sci U S A *101*, 9988-9993.
Cai, M.Y., Dunn, C.E., Chen, W., Kochupurakkal, B.S., Nguyen, H., Moreau, L.A., Shapiro, G.I., Parmar, K., Kozono, D., and D'Andrea, A.D. (2020). Cooperation of the ATM and Fanconi Anemia/BRCA Pathways in Double-Strand Break End Resection. Cell Rep *30*, 2402-2415 e2405.
Carr, A.M., and Lambert, S. (2013). Replication stress-induced genome instability: the dark side of replication maintenance by homologous recombination. J Mol Biol *425*, 4733-4744.
Carreira, A., Hilario, J., Amitani, I., Baskin, R.J., Shivji, M.K., Venkitaraman, A.R., and Kowalczykowski, S.C. (2009). The BRC repeats of BRCA2 modulate the DNA-binding selectivity of RAD51. Cell *136*, 1032-1043.
Carreira, A., and Kowalczykowski, S.C. (2011). Two classes of BRC repeats in BRCA2 promote RAD51 nucleoprotein filament function by distinct mechanisms. Proc Natl Acad Sci U S A *108*, 10448-10453.
Ceccaldi, R., Liu, J.C., Amunugama, R., Hajdu, I., Primack, B., Petalcorin, M.I., O'Connor, K.W., Konstantinopoulos, P.A., Elledge, S.J., Boulton, S.J.*, et al.* (2015). Homologous-recombination-deficient tumours are dependent on Poltheta-mediated repair. Nature *518*, 258-262.
Cejka, P. (2021). Single-molecule studies illuminate the function of RAD51 paralogs. Mol Cell *81*, 898-900.
Cejka, P., Cannavo, E., Polaczek, P., Masuda-Sasa, T., Pokharel, S., Campbell, J.L., and Kowalczykowski, S.C. (2010). DNA end resection by Dna2-Sgs1-RPA and its stimulation by Top3-Rmi1 and Mre11-Rad50-Xrs2. Nature *467*, 112-116.
Ceppi, I., Howard, S.M., Kasaciunaite, K., Pinto, C., Anand, R., Seidel, R., and Cejka, P. (2020). CtIP promotes the motor activity of DNA2 to accelerate long-range DNA end resection. Proc Natl Acad Sci U S A *117*, 8859-8869.
Chaudhury, I., Sareen, A., Raghunandan, M., and Sobeck, A. (2013). FANCD2 regulates BLM complex functions independently of FANCI to promote replication fork recovery. Nucleic Acids Res *41*, 6444-6459.
Chaudhury, I., Stroik, D.R., and Sobeck, A. (2014). FANCD2-controlled chromatin access of the Fanconi-associated nuclease FAN1 is crucial for the recovery of stalled replication forks. Mol Cell Biol *34*, 3939-3954.
Chen, X., Bosques, L., Sung, P., and Kupfer, G.M. (2017). A novel role for non-ubiquitinated FANCD2 in response to hydroxyurea-induced DNA damage. Oncogene *36*, 5220.
Colosio, A., Frattini, C., Pellicano, G., Villa-Hernandez, S., and Bermejo, R. (2016). Nucleolytic processing of aberrant replication intermediates by an Exo1-Dna2-Sae2 axis counteracts fork

collapse-driven chromosome instability. Nucleic Acids Res *44*, 10676-10690.
Cong, K., Kousholt, A.N., Peng, M., Panzarino, N.J., Lee, W.T.C., Nayak, S., Krais, J., Calvo, J., Bere, M., Rothenberg, E.*, et al.* (2019). PARPi synthetic lethality derives from replication-associated single-stranded DNA gaps. BioRxiv.
Couch, F.B., Bansbach, C.E., Driscoll, R., Luzwick, J.W., Glick, G.G., Betous, R., Carroll, C.M., Jung, S.Y., Qin, J., Cimprich, K.A.*, et al.* (2013). ATR phosphorylates SMARCAL1 to prevent replication fork collapse. Genes Dev *27*, 1610-1623.
Diffley, J.F. (2020). BioRxiv.
Dubois, E.L., Guitton-Sert, L., Beliveau, M., Parmar, K., Chagraoui, J., Vignard, J., Pauty, J., Caron, M.C., Coulombe, Y., Buisson, R.*, et al.* (2019). A Fanci knockout mouse model reveals common and distinct functions for FANCI and FANCD2. Nucleic Acids Res *47*, 7532-7547.
Dungrawala, H., Rose, K.L., Bhat, K.P., Mohni, K.N., Glick, G.G., Couch, F.B., and Cortez, D. (2015). The Replication Checkpoint Prevents Two Types of Fork Collapse without Regulating Replisome Stability. Mol Cell *59*, 998-1010.
Duxin, J.P., and Walter, J.C. (2015). What is the DNA repair defect underlying Fanconi anemia? Curr Opin Cell Biol *37*, 49-60.
Federico, M.B., Campodonico, P., Paviolo, N.S., and Gottifredi, V. (2018). Beyond interstrand crosslinks repair: contribution of FANCD2 and other Fanconi Anemia proteins to the replication of DNA. Mutat Res *808*, 83-92.
Fumasoni, M., Zwicky, K., Vanoli, F., Lopes, M., and Branzei, D. (2015). Error-free DNA damage tolerance and sister chromatid proximity during DNA replication rely on the Polalpha/Primase/Ctf4 Complex. Mol Cell *57*, 812-823.
Hanzlikova, H., Kalasova, I., Demin, A.A., Pennicott, L.E., Cihlarova, Z., and Caldecott, K.W. (2018). The Importance of Poly(ADP-Ribose) Polymerase as a Sensor of Unligated Okazaki Fragments during DNA Replication. Mol Cell *71*, 319-331 e313.
Hashimoto, Y., Chaudhuri, A.R., Lopes, M., and Costanzo, V. (2010). Rad51 protects nascent DNA from Mre11-dependent degradation and promotes continuous DNA synthesis. Nat Struct Mol Biol *17*, 1305-1311.
Hashimoto, Y., Puddu, F., and Costanzo, V. (2012). RAD51- and MRE11-dependent reassembly of uncoupled CMG helicase complex at collapsed replication forks. Nat Struct Mol Biol *19*, 17-24.
Helleday, T., Petermann, E., Lundin, C., Hodgson, B., and Sharma, R.A. (2008). DNA repair pathways as targets for cancer therapy. Nat Rev Cancer *8*, 193-204.
Higgins, N.P., Kato, K., and Strauss, B. (1976). A model for replication repair in mammalian cells. J Mol Biol *101*, 417-425.
Higgs, M.R., Reynolds, J.J., Winczura, A., Blackford, A.N., Borel, V., Miller, E.S., Zlatanou, A., Nieminuszczy, J., Ryan, E.L., Davies, N.J.*, et al.* (2015). BOD1L Is Required to Suppress Deleterious Resection of Stressed Replication Forks. Mol Cell *59*, 462-477.

Higgs, M.R., Sato, K., Reynolds, J.J., Begum, S., Bayley, R., Goula, A., Vernet, A., Paquin, K.L., Skalnik, D.G., Kobayashi, W.*, et al.* (2018). Histone Methylation by SETD1A Protects Nascent DNA through the Nucleosome Chaperone Activity of FANCD2. Mol Cell *71*, 25-41 e26.

Higgs, M.R., and Stewart, G.S. (2016). Protection or resection: BOD1L as a novel replication fork protection factor. Nucleus *7*, 34-40.

Hoa, N.N., Kobayashi, J., Omura, M., Hirakawa, M., Yang, S.H., Komatsu, K., Paull, T.T., Takeda, S., and Sasanuma, H. (2015). BRCA1 and CtIP Are Both Required to Recruit Dna2 at Double-Strand Breaks in Homologous Recombination. PLoS One *10*, e0124495.

Hu, J., Sun, L., Shen, F., Chen, Y., Hua, Y., Liu, Y., Zhang, M., Hu, Y., Wang, Q., Xu, W.*, et al.* (2012). The intra-s phase checkpoint targets dna2 to prevent stalled replication forks from reversing. Cell *149*, 1221-1232.

Jensen, R.B., Carreira, A., and Kowalczykowski, S.C. (2010). Purified human BRCA2 stimulates RAD51-mediated recombination. Nature *467*, 678-683.

Jiang, Q., Paramasivam, M., Aressy, B., Wu, J., Bellani, M., Tong, W., Seidman, M.M., and Greenberg, R.A. (2015). MERIT40 cooperates with BRCA2 to resolve DNA interstrand cross-links. Genes Dev.

Kais, Z., Rondinelli, B., Holmes, A., O'Leary, C., Kozono, D., D'Andrea, A.D., and Ceccaldi, R. (2016). FANCD2 Maintains Fork Stability in BRCA1/2-Deficient Tumors and Promotes Alternative End-Joining DNA Repair. Cell Rep *15*, 2488-2499.

Karanja, K.K., Lee, E.H., Hendrickson, E.A., and Campbell, J.L. (2014). Preventing over-resection by DNA2 helicase/nuclease suppresses repair defects in Fanconi anemia cells. Cell Cycle *13*, 1540-1550.

Karanja, K.K., S.W., C., Duxin, J.P., Stewart, S.A., and Campbell, J.L. (2012). DNA2 and EXO1 in Replication-coupled Homology Directed Repair and in the Interplay Between HDR and the FA/BRCA Network. Cell Cycle *11*, 3983-3996.

Knipscheer, P., Raschle, M., Smogorzewska, A., Enoiu, M., Ho, T.V., Scharer, O.D., Elledge, S.J., and Walter, J.C. (2009). The Fanconi anemia pathway promotes replication-dependent DNA interstrand cross-link repair. Science *326*, 1698-1701.

Kolinjivadi, A.M., Sannino, V., de Antoni, A., Techer, H., Baldi, G., and Costanzo, V. (2017a). Moonlighting at replication forks - a new life for homologous recombination proteins BRCA1, BRCA2 and RAD51. FEBS Lett *591*, 1083-1100.

Kolinjivadi, A.M., Sannino, V., De Antoni, A., Zadorozhny, K., Kilkenny, M., Techer, H., Baldi, G., Shen, R., Ciccia, A., Pellegrini, L.*, et al.* (2017b). Smarcal1-Mediated Fork Reversal Triggers Mre11-Dependent Degradation of Nascent DNA in the Absence of Brca2 and Stable Rad51 Nucleofilaments. Mol Cell *67*, 867-881 e867.

Kottemann, M.C., and Smogorzewska, A. (2013). Fanconi anaemia and the repair of Watson and Crick DNA crosslinks. Nature *493*, 356-363.

Kumar, S., Peng, X., Daley, J., Yang, L., Shen, J., Nguyen, N., Bae, G., Niu, H., Peng, Y., Hsieh, H.J.*, et al.* (2017). Inhibition of DNA2 nuclease as a therapeutic strategy targeting replication stress in cancer cells. Oncogenesis *6*, e319.

Lachaud, C., and Rouse, J. (2016). A route to new cancer therapies: the FA pathway is essential in BRCA1- or BRCA2-deficient cells. Nat Struct Mol Biol *23*, 701-703.

Lemacon, D., Jackson, J., Quinet, A., Brickner, J.R., Li, S., Yazinski, S., You, Z., Ira, G., Zou, L., Mosammaparast, N.*, et al.* (2017). MRE11 and EXO1 nucleases degrade reversed forks and elicit MUS81-dependent fork rescue in BRCA2-deficient cells. Nat Commun *8*, 860.

Lin, W., Sampathi, S., Dai, H., Liu, C., Zhou, M., Hu, J., Huang, Q., Campbell, J., Shin-Ya, K., Zheng, L.*, et al.* (2013). Mammalian DNA2 helicase/nuclease cleaves G-quadruplex DNA and is required for telomere integrity. EMBO J *32*, 1425-1439.

Liu, J., Renault, L., Veaute, X., Fabre, F., Stahlberg, H., and Heyer, W.D. (2011). Rad51 paralogues Rad55-Rad57 balance the antirecombinase Srs2 in Rad51 filament formation. Nature *479*, 245-248.

Liu, W., Krishnamoorthy, A., Zhao, R., and Cortez, D. (2020). Two replication fork remodeling pathways generate nuclease substrates for distinct fork protection factors. Sci Adv *6*.

Liu, W., Zhou, M., Li, Z., Li, H., Polaczek, P., Dai, H., Wu, Q., Liu, C., Karanja, K.K., Popuri, V.*, et al.* (2016). A Selective Small Molecule DNA2 Inhibitor for Sensitization of Human Cancer Cells to Chemotherapy. EBioMedicine *6*, 73-86.

Long, D.T., Joukov, V., Budzowska, M., and Walter, J.C. (2014). BRCA1 promotes unloading of the CMG helicase from a stalled DNA replication fork. Mol Cell *56*, 174-185.

Long, D.T., Raschle, M., Joukov, V., and Walter, J.C. (2011). Mechanism of RAD51-dependent DNA interstrand cross-link repair. Science *333*, 84-87.

Long, D.T., and Walter, J.C. (2012). A novel function for BRCA1 in crosslink repair. Mol Cell *46*, 111-112.

Lossaint, G., Larroque, M., Ribeyre, C., Bec, N., Larroque, C., Decaillet, C., Gari, K., and Constantinou, A. (2013). FANCD2 Binds MCM Proteins and Controls Replisome Function upon Activation of S Phase Checkpoint Signaling. Mol Cell *51*, 678-690.

Masuda-Sasa, T., Imamura, O., and Campbell, J.L. (2006). Biochemical analysis of human Dna2. Nucleic Acids Res *34*, 1865-1875.

Maya-Mendoza, A., Moudry, P., Merchut-Maya, J.M., Lee, M., Strauss, R., and Bartek, J. (2018). High speed of fork progression induces DNA replication stress and genomic instability. Nature *559*, 279-284.

Mazina, O.M., Keskin, H., Hanamshet, K., Storici, F., and Mazin, A.V. (2017). Rad52 Inverse Strand Exchange Drives RNA-Templated DNA Double-Strand Break Repair. Mol Cell *67*, 19-29 e13.

Merchut-Maya, J.M., Bartek, J., and Maya-Mendoza, A. (2019). Regulation of replication fork speed: Mechanisms and impact on genomic stability. DNA Repair (Amst) *81*, 102654.

Michl, J., Zimmer, J., Buffa, F.M., McDermott, U., and Tarsounas, M. (2016). FANCD2 limits replication stress and genome instability in cells lacking BRCA2. Nat Struct Mol Biol *23*, 755-757.

Mijic, S., Zellweger, R., Chappidi, N., Berti, M., Jacobs, K., Mutreja, K., Ursich, S., Ray Chaudhuri, A., Nussenzweig, A., Janscak, P.*, et al.* (2017). Replication fork reversal triggers fork degradation in BRCA2-defective cells. Nat Commun *8*, 859.

Murina, O., von Aesch, C., Karakus, U., Ferretti, L.P., Bolck, H.A., Hanggi, K., and Sartori, A.A. (2014). FANCD2 and CtIP cooperate to repair DNA interstrand crosslinks. Cell Rep *7*, 1030-1038.

Nakanishi, K., Cavallo, F., Brunet, E., and Jasin, M. (2011). Homologous recombination assay for interstrand cross-link repair. Methods Mol Biol *745*, 283-291.

Nimonkar, A.V., Genschel, J., Kinoshita, E., Polaczek, P., Campbell, J.L., Wyman, C., Modrich, P., and Kowalczykowski, S.C. (2011). BLM-DNA2-RPA-MRN- and EXO1-BLM-RPA-MRN constitute two DNA end resection machineries for human DNA break repair. Genes Dev *25*, 350-362.

Niraj, J., Caron, M.C., Drapeau, K., Berube, S., Guitton-Sert, L., Coulombe, Y., Couturier, A.M., and Masson, J.Y. (2017). The identification of FANCD2 DNA binding domains reveals nuclear localization sequences. Nucleic Acids Res *45*, 8341-8357.

Pace, P., Mosedale, G., Hodskinson, M.R., Rosado, I.V., Sivasubramaniam, M., and Patel, K.J. (2010). Ku70 corrupts DNA repair in the absence of the Fanconi anemia pathway. Science *329*, 219-223.

Panzarino, N.J., Krais, J., Peng, M., Mosqueda, M., Nayak, S., Bond, S., Calvo, J., Cong, K., Doshi, M., Bere, M.*, et al.* (2019). Replication gaps underlie BRCA-deficiency and therapy response. BioRxiv.

Paull, T.T., and Gellert, M. (1998). The 3' to 5' exonuclease activity of Mre11 facilitates repair of DNA double-strand breaks. Mol. Cell *1*, 969-979.

Petermann, E., Orta, M.L., Issaeva, N., Schultz, N., and Helleday, T. (2010). Hydroxyurea-stalled replication forks become progressively inactivated and require two different RAD51-mediated pathways for restart and repair. Mol Cell *37*, 492-502.

Piberger, A.L., Walker, A.K., Morris, J.R., Bryant, H., and Petermann, E. (2019). PrimPol-dependent single-stranded gap formation mediates homologous recombination at bulky DNA adducts. BioRxiv.

Piwko, W., Mlejnkova, L.J., Mutreja, K., Ranjha, L., Stafa, D., Smirnov, A., Brodersen, M.M., Zellweger, R., Sturzenegger, A., Janscak, P.*, et al.* (2016). The MMS22L-TONSL heterodimer directly promotes RAD51-dependent recombination upon replication stress. EMBO J *35*, 2584-2601.

Quinet, A., Lemacon, D., and Vindigni, A. (2017). Replication Fork Reversal: Players and Guardians. Mol Cell *68*, 830-833.

Quinet, A., Tirman, S., Jackson, J., Svikovic, S., Lemacon, D., Carvajal-Maldonado, D., Gonzalez-Acosta, D., Vessoni, A.T., Cybulla, E., Wood, M.*, et al.* (2019). PRIMPOL-Mediated Adaptive Response Suppresses Replication Fork Reversal in BRCA-Deficient Cells. Mol Cell.
Raghunandan, M., Chaudhury, I., Kelich, S.L., Hanenberg, H., and Sobeck, A. (2015). FANCD2, FANCJ and BRCA2 cooperate to promote replication fork recovery independently of the Fanconi Anemia core complex. Cell Cycle *14*, 342-353.
Raschle, M., Knipscheer, P., Enoiu, M., Angelov, T., Sun, J., Griffith, J.D., Ellenberger, T.E., Scharer, O.D., and Walter, J.C. (2008). Mechanism of replication-coupled DNA interstrand crosslink repair. Cell *134*, 969-980.
Ray Chaudhuri, A., Ahuja, A.K., Herrador, R., and Lopes, M. (2015). Poly(ADP-Ribosyl) glycohydrolase prevents the accumulation of unusual replication structures during unperturbed S phase. Mol Cell Biol *35*, 856-865.
Ray Chaudhuri, A., Callen, E., Ding, X., Gogola, E., Duarte, A.A., Lee, J.E., Wong, N., Lafarga, V., Calvo, J.A., Panzarino, N.J.*, et al.* (2016). Replication fork stability confers chemoresistance in BRCA-deficient cells. Nature *535*, 382-387.
Ray Chaudhuri, A., Hashimoto, Y., Herrador, R., Neelsen, K.J., Fachinetti, D., Bermejo, R., Cocito, A., Costanzo, V., and Lopes, M. (2012). Topoisomerase I poisoning results in PARP-mediated replication fork reversal. Nat Struct Mol Biol *19*, 417-423.
Rennie, M.L., Lemonidis, K., Arkinson, C., Chaugule, V.K., Clarke, M., Streetley, J., Spagnolo, L., and Walden, H. (2020). Differential functions of FANCI and FANCD2 ubiquitination stabilize ID2 complex on DNA. EMBO Rep *21*, e50133.
Rickman, K.A., Noonan, R.J., Lach, F.P., Sridhar, S., Wang, A.T., Abhyankar, A., Huang, A., Kelly, M., Auerbach, A.D., and Smogorzewska, A. (2020). Distinct roles of BRCA2 in replication fork protection in response to hydroxyurea and DNA interstrand cross-links. Genes Dev *34*, 832-846.
Roques, C., Coulombe, Y., Delannoy, M., Vignard, J., Grossi, S., Brodeur, I., Rodrigue, A., Gautier, J., Stasiak, A.Z., Stasiak, A.*, et al.* (2009). MRE11-RAD50-NBS1 is a critical regulator of FANCD2 stability and function during DNA double-strand break repair. EMBO J *28*, 2400-2413.
Roy, U., Kwon, Y., Marie, L., Symington, L., Sung, P., Lisby, M., and Greene, E.C. (2021). The Rad51 paralog complex Rad55-Rad57 acts as a molecular chaperone during homologous recombination. Mol Cell *81*, 1043-1057 e1048.
Sato, K., Shimomuki, M., Katsuki, Y., Takahashi, D., Kobayashi, W., Ishiai, M., Miyoshi, H., Takata, M., and Kurumizaka, H. (2016). FANCI-FANCD2 stabilizes the RAD51-DNA complex by binding RAD51 and protects the 5'-DNA end. Nucleic Acids Res *44*, 10758-10771.
Schlacher, K., Christ, N., Siaud, N., Egashira, A., Wu, H., and Jasin, M. (2011). Double-strand break repair-independent role for BRCA2 in blocking stalled replication fork degradation by MRE11. Cell *145*, 529-542.

Schlacher, K., Wu, H., and Jasin, M. (2012). A Distinct Replication Fork Protection Pathway Connects Fanconi Anemia Tumor Suppressors to RAD51-BRCA1/2. Cancer Cell *22*, 106-116.
Shao, H., Baitinger, C., Soderblom, E.J., Burdett, V., and Modrich, P. (2014). Hydrolytic function of Exo1 in mammalian mismatch repair. Nucleic Acids Res *42*, 7104-7112.
Shibata, A., Moiani, D., Arvai, A.S., Perry, J., Harding, S.M., Genols, M.-M., Maity, R., Rossum-Fikkert, S.v., Kertokallo, A., Romoli, F.*, et al.* (2014). DNA Double-Strand Break Repair Pathway Choice is Directed by Distinct MRE11 Nuclease Activities. Mol Cell *53*, 7-18.
Sobeck, A., Stone, S., Costanzo, V., de Graaf, B., Reuter, T., de Winter, J., Wallisch, M., Akkari, Y., Olson, S., Wang, W.*, et al.* (2006). Fanconi anemia proteins are required to prevent accumulation of replication-associated DNA double-strand breaks. Mol Cell Biol *26*, 425-437.
Sullivan, M.R., and Bernstein, K.A. (2018). RAD-ical New Insights into RAD51 Regulation. Genes (Basel) *9*.
Symington, L.S., and Gautier, J. (2011). Double-Strand Break End Resection and Repair Pathway Choice. Annu Rev Genet.
Taglialatela, A., Alvarez, S., Leuzzi, G., Sannino, V., Ranjha, L., Huang, J.W., Madubata, C., Anand, R., Levy, B., Rabadan, R.*, et al.* (2017). Restoration of Replication Fork Stability in BRCA1- and BRCA2-Deficient Cells by Inactivation of SNF2-Family Fork Remodelers. Mol Cell *68*, 414-430 e418.
Takahashi, D., Sato, K., Shimomuki, M., Takata, M., and Kurumizaka, H. (2014). Expression and purification of human FANCI and FANCD2 using Escherichia coli cells. Protein Expr Purif *103*, 8-15.
Tan, W., van Twest, S., Leis, A., Bythell-Douglas, R., Murphy, V.J., Sharp, M., Parker, M.W., Crismani, W., and Deans, A.J. (2020). Monoubiquitination by the human Fanconi anemia core complex clamps FANCI:FANCD2 on DNA in filamentous arrays. Elife *9*.
Taylor, J.H. (1958). The mode of chromosome duplication in *Crepis capillaris*. Exp. Cell Res. *15*, 350-357.
Taylor, M.R.G., Spirek, M., Chaurasiya, K.R., Ward, J.D., Carzaniga, R., Yu, X., Egelman, E.H., Collinson, L.M., Rueda, D., Krejci, L.*, et al.* (2015). Rad51 Paralogs Remodel Pre-synaptic Rad51 Filaments to Stimulate Homologous Recombination. Cell *162*, 271-286.
Thakar, T., Leung, W., Nicolae, C.M., Clements, K.E., Binghui Shen, Bielinsky, A.-K., and Moldovan, G.-L. (2019). PCNA ubiquitination protects stalled replication forks from DNA2-mediated degradation by regulating Okazaki fragment maturation and chromatin assembly . BioRxiv.
Thangavel, S., Berti, M., Levikova, M., Pinto, C., Gomathinayagam, S., Vujanovic, M., Zellweger, R., Moore, H., Lee, E.H., Hendrickson, E.A.*, et al.* (2015). DNA2 drives processing and restart of reversed replication forks in human cells. J Cell Biol *208*, 545-562.
Thangavel, S., Mendoza-Maldonado, R., Tissino, E., Sidorova, J.M., Yin, J., Wang, W., Monnat, R.J., Jr., Falaschi, A., and Vindigni, A. (2010). Human RECQ1 and RECQ4 helicases play

distinct roles in DNA replication initiation. Mol Cell Biol *30*, 1382-1396.
Thompson, E.L., Yeo, J.E., Lee, E.A., Kan, Y., Raghunandan, M., Wiek, C., Hanenberg, H., Scharer, O.D., Hendrickson, E.A., and Sobeck, A. (2017). FANCI and FANCD2 have common as well as independent functions during the cellular replication stress response. Nucleic Acids Res *45*, 11837-11857.
Thorslund, T., McIlwraith, M.J., Compton, S.A., Lekomtsev, S., Petronczki, M., Griffith, J.D., and West, S.C. (2010). The breast cancer tumor suppressor BRCA2 promotes the specific targeting of RAD51 to single-stranded DNA. Nat Struct Mol Biol *17*, 1263-1265.
Tian, Y., Shen, X., Wang, R., Klages-Mundt, N.L., Lynn, E.J., Martin, S.K., Ye, Y., Gao, M., Chen, J., Schlacher, K.*, et al.* (2017). Constitutive role of the Fanconi anemia D2 gene in the replication stress response. J Biol Chem *292*, 20184-20195.
Timmers, C., Taniguchi, T., Hejna, J., Reifsteck, C., Lucas, L., Bruun, D., Thayer, M., Cox, B., Olson, S., D'Andrea, A.D.*, et al.* (2001). Positional cloning of a novel Fanconi anemia gene, FANCD2. Mol Cell *7*, 241-248.
Unno, J., Itaya, A., Taoka, M., Sato, K., Tomida, J., Sakai, W., Sugasawa, K., Ishiai, M., Ikura, T., Isobe, T.*, et al.* (2014). FANCD2 binds CtIP and regulates DNA-end resection during DNA interstrand crosslink repair. Cell Rep *7*, 1039-1047.
van Gool, A.J., Shah, R., Mezard, C., and West, S.C. (1998). Functional interactions between the holliday junction resolvase and the branch migration motor of Escherichia coli. EMBO J *17*, 1838-1845.
Velimezi, G., Robinson-Garcia, L., Munoz-Martinez, F., Wiegant, W.W., Ferreira da Silva, J., Owusu, M., Moder, M., Wiedner, M., Rosenthal, S.B., Fisch, K.M.*, et al.* (2018). Map of synthetic rescue interactions for the Fanconi anemia DNA repair pathway identifies USP48. Nat Commun *9*, 2280.
Vujanovic, M., Krietsch, J., Raso, M.C., Terraneo, N., Zellweger, R., Schmid, J.A., Taglialatela, A., Huang, J.W., Holland, C.L., Zwicky, K.*, et al.* (2017). Replication Fork Slowing and Reversal upon DNA Damage Require PCNA Polyubiquitination and ZRANB3 DNA Translocase Activity. Mol Cell *67*, 882-890 e885.
Wang, A.T., Kim, T., Wagner, J.E., Conti, B.A., Lach, F.P., Huang, A.L., Molina, H., Sanborn, E.M., Zierhut, H., Cornes, B.K.*, et al.* (2015). A Dominant Mutation in Human RAD51 Reveals Its Function in DNA Interstrand Crosslink Repair Independent of Homologous Recombination. Mol Cell *59*, 478-490.
Wang, R., Wang, S., Dhar, A., Peralta, C., and Pavletich, N.P. (2020). DNA clamp function of the monoubiquitinated Fanconi anaemia ID complex. Nature *580*, 278-282.
Whelan, D.R., and Rothenberg, E. (2021). Super-resolution mapping of cellular double-strand break resection complexes during homologous recombination. Proc Natl Acad Sci U S A *118*.
Yang, W. (2011). Nucleases: diversity of structure, function and mechanism. Q Rev Biophys *44*, 1-93.

Yeo, J.E., Lee, E.H., Hendrickson, E.A., and Sobeck, A. (2014). CtIP mediates replication fork recovery in a FANCD2-regulated manner. Hum Mol Genet *23*, 3695-3705.

Zadorozhny, K., Sannino, V., Belan, O., Mlcouskova, J., Spirek, M., Costanzo, V., and Krejci, L. (2017). Fanconi-Anemia-Associated Mutations Destabilize RAD51 Filaments and Impair Replication Fork Protection. Cell Rep *21*, 333-340.

Zellweger, R., Dalcher, D., Mutreja, K., Berti, M., Schmid, J.A., Herrador, R., Vindigni, A., and Lopes, M. (2015). Rad51-mediated replication fork reversal is a global response to genotoxic treatments in human cells. J Cell Biol *208*, 563-579.

Zhang, Y., and Jasin, M. (2011). An essential role for CtIP in chromosomal translocation formation through an alternative end-joining pathway. Nat Struct Mol Biol *18*, 80-84.

Zheng, L., Meng, Y., Campbell, J.L., and Shen, B. (2020). Multiple roles of DNA2 nuclease/helicase in DNA metabolism, genome stability and human diseases. Nucleic Acids Res *48*, 16-35.

Figure 1

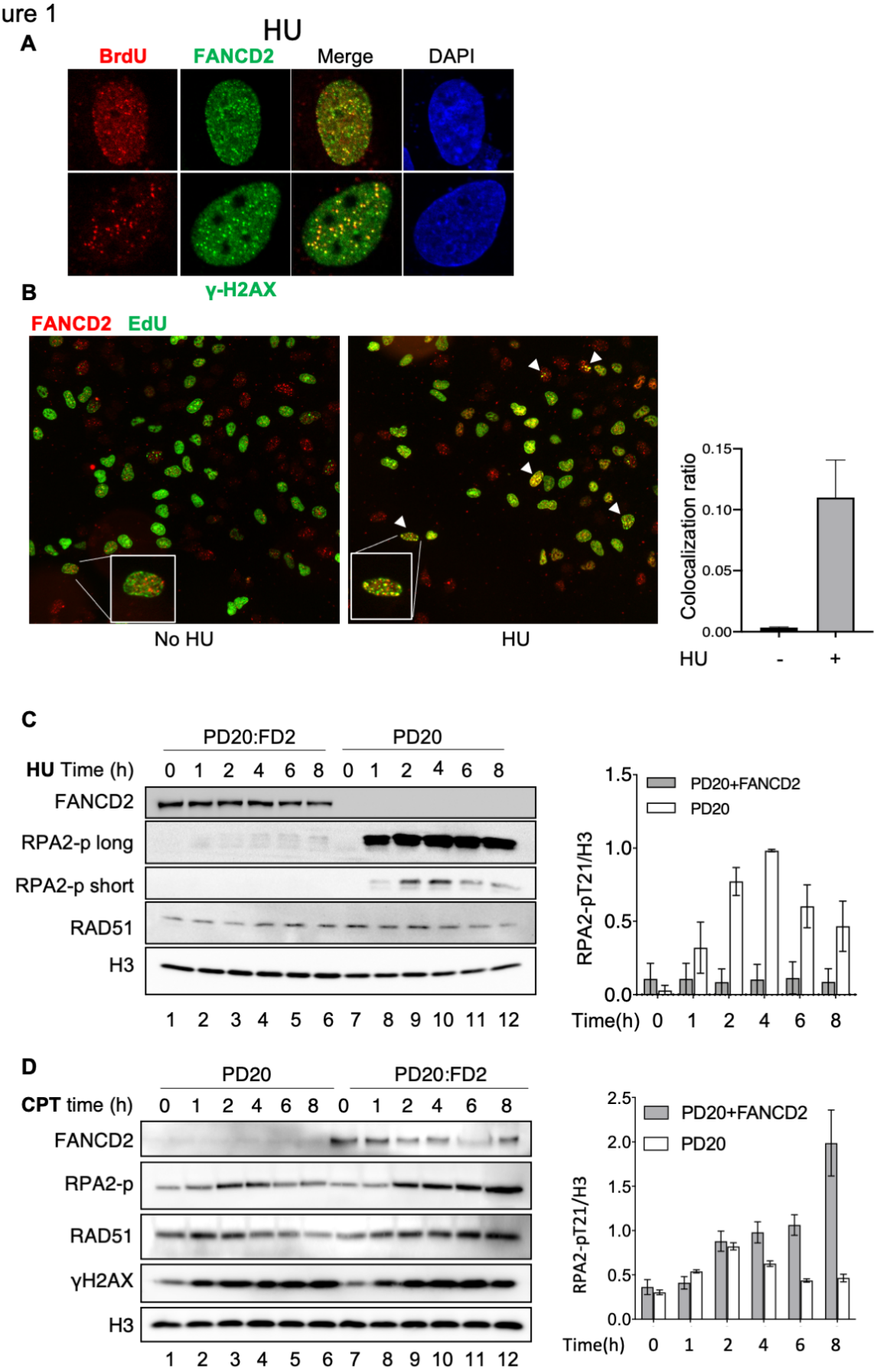
A
HU
BrdU
FANCD2
Merge
DAPI
γ-H2AX
B
FANCD2 EdU
No HU
HU
Colocalization ratio
0.15
0.10
0.05
0.00
HU - +
C
PD20:FD2
PD20
HU Time (h) 0 1 2 4 6 8 0 1 2 4 6 8
FANCD2
RPA2-p long
RPA2-p short
RAD51
H3
1 2 3 4 5 6 7 8 9 10 11 12
PD20+FANCD2
PD20
RPA2-pT21/H3
1.5
1.0
0.5
0.0
Time(h) 0 1 2 4 6 8
D
PD20
PD20:FD2
CPT time (h) 0 1 2 4 6 8 0 1 2 4 6 8
FANCD2
RPA2-p
RAD51
γH2AX
H3
1 2 3 4 5 6 7 8 9 10 11 12
PD20+FANCD2
PD20
RPA2-pT21/H3
2.5
2.0
1.5
1.0
0.5
0.0
Time(h) 0 1 2 4 6 8

Figure 1. FANCD2 has two different roles at stalled replication forks depending on extent of stalling.

(A) γH2AX and FANCD2 show co-localization with BrdU in response to HU. A549 cells were treated with 150 μM BrdU for 20 minutes, and then HU was added for 30 mins(Couch et al., 2013). Cells were prepared for immunofluorescence under native conditions as indicated in Method Details. Cells were stained with α-BrdU and α-γH2AX antibodies or α-BrdU and FANCD2 antibodies as indicated in the figure and imaged: anti-BrdU, red; α-γH2AX, green; α-FANCD2 green; DAPI, blue (DNA).

(B) FANCD2 co-localizes with nascent DNA after fork stalling. U2OS cells were labeled with 10μM EdU for 10 minutes. Then 4mM HU was added after EdU labeling for 2 hours. Then the U2OS cells were prepared for immunofluorescence together with non-HU condition. The number of cells with greater than 4 foci that showed colocalization of FANCD2 (red) and EdU (green) were counted, and the ratio of the number of cells with colocalized foci over total cells determined and plotted. Over 800 cells were counted for each. Error was derived from standard deviation from two independent experiments.

(C) FANCD2 prevents resection in response to HU. PD20 cells and PD20:FANCD2 complemented cells treated with 3 mM hydroxyurea for 0-8 hours. HU was added and samples were taken at 0, 2, 4, 6, and 8 h. Nuclear extract was prepared, as illustrated by the H3 loading control, and analyzed for resection by western blot. “RPA2-p long” refers to long exposure time monitoring RPA2 T21 phosphorylation; “RPA2-short” is a short exposure time monitoring RPA2 T21 phosphorylation. The RPA2-p and histone H3 blot intensity were measured with ImageJ. Then RPA2-p value was normalized to histone H3. The graph value is the average of two experiments; error bar is standard deviation.

(D) PD20 FANCD2$^{-/-}$ cell and PD20 complemented with FANCD2 (PD20:FD2) were treated with 2 μM CPT for indicated times. Nuclear extract was prepared and used for the western blots for proteins and protein modifications as indicated in the figure.

Figure 2

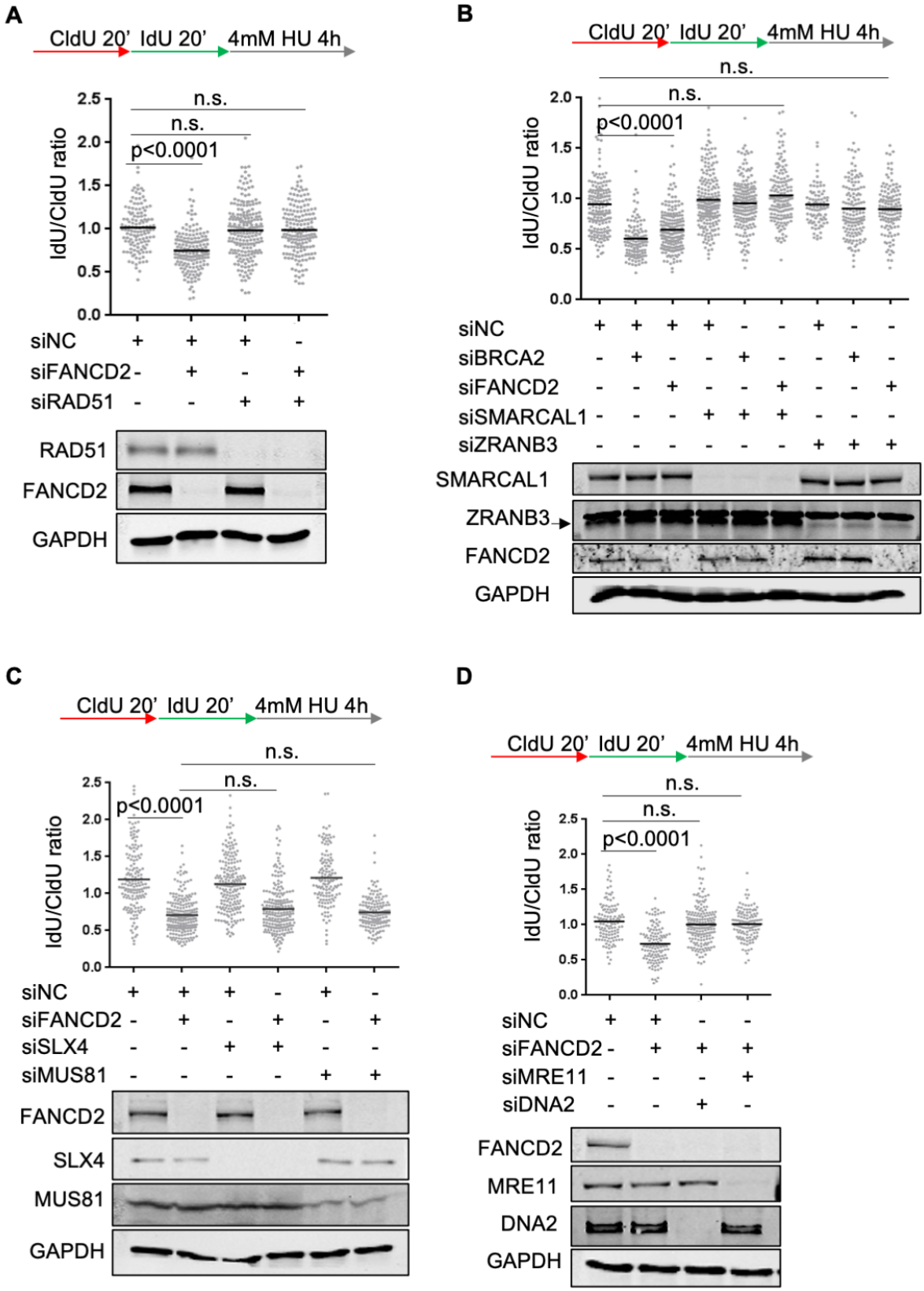
A
CldU 20' IdU 20' 4mM HU 4h
IdU/CldU ratio
n.s.
n.s.
p<0.0001
siNC
siFANCD2
siRAD51
RAD51
FANCD2
GAPDH
B
CldU 20' IdU 20' 4mM HU 4h
IdU/CldU ratio
n.s.
n.s.
p<0.0001
siNC
siBRCA2
siFANCD2
siSMARCAL1
siZRANB3
SMARCAL1
ZRANB3
FANCD2
GAPDH
C
CldU 20' IdU 20' 4mM HU 4h
IdU/CldU ratio
n.s.
n.s.
p<0.0001
siNC
siFANCD2
siSLX4
siMUS81
FANCD2
SLX4
MUS81
GAPDH
D
CldU 20' IdU 20' 4mM HU 4h
IdU/CldU ratio
n.s.
n.s.
p<0.0001
siNC
siFANCD2
siMRE11
siDNA2
FANCD2
MRE11
DNA2
GAPDH

Figure 2. FANCD2 Prevents Nascent DNA Degradation at Reversed Forks and Depletion of DNA2 or Mre11 Prevents Over-resection.

U2OS cells were co-transfected with 12 nM siRNA for each indicated gene. 72 hours post-transfection, as indicated on the top of the panel, cells were pulsed by CldU and IdU, followed by 4 mM HU for 4h. The cells were harvested and analyzed by fiber spreading assay. The IdU and CldU tract lengths were measured, and the ratio was graphed (≥150 fibers were analyzed). One-way ANOVA test was performed, n=2. Western blots show quantification of knockdown.

(A) Unrestrained nascent DNA resection in HU-treated FANCD2 deficient cells is rescued by depletion of RAD51. Western blots in panels a-d show efficiency of knockdown.

(B) Over-resection of nascent DNA in HU-treated FANCD2 deficient cells is fork reversal dependent. The arrow in the western blot beside ZRANB3 indicates the ZRANB3 protein band.

(C) Over-resection of nascent DNA in HU-treated FANCD2 deficient cells is not reduced by depletion of SLX4 or MUS81.

(D) Over-resection of nascent DNA in HU-treated FANCD2 deficient cells is reduced by either DNA2 or MRE11 depletion.

Figure 3

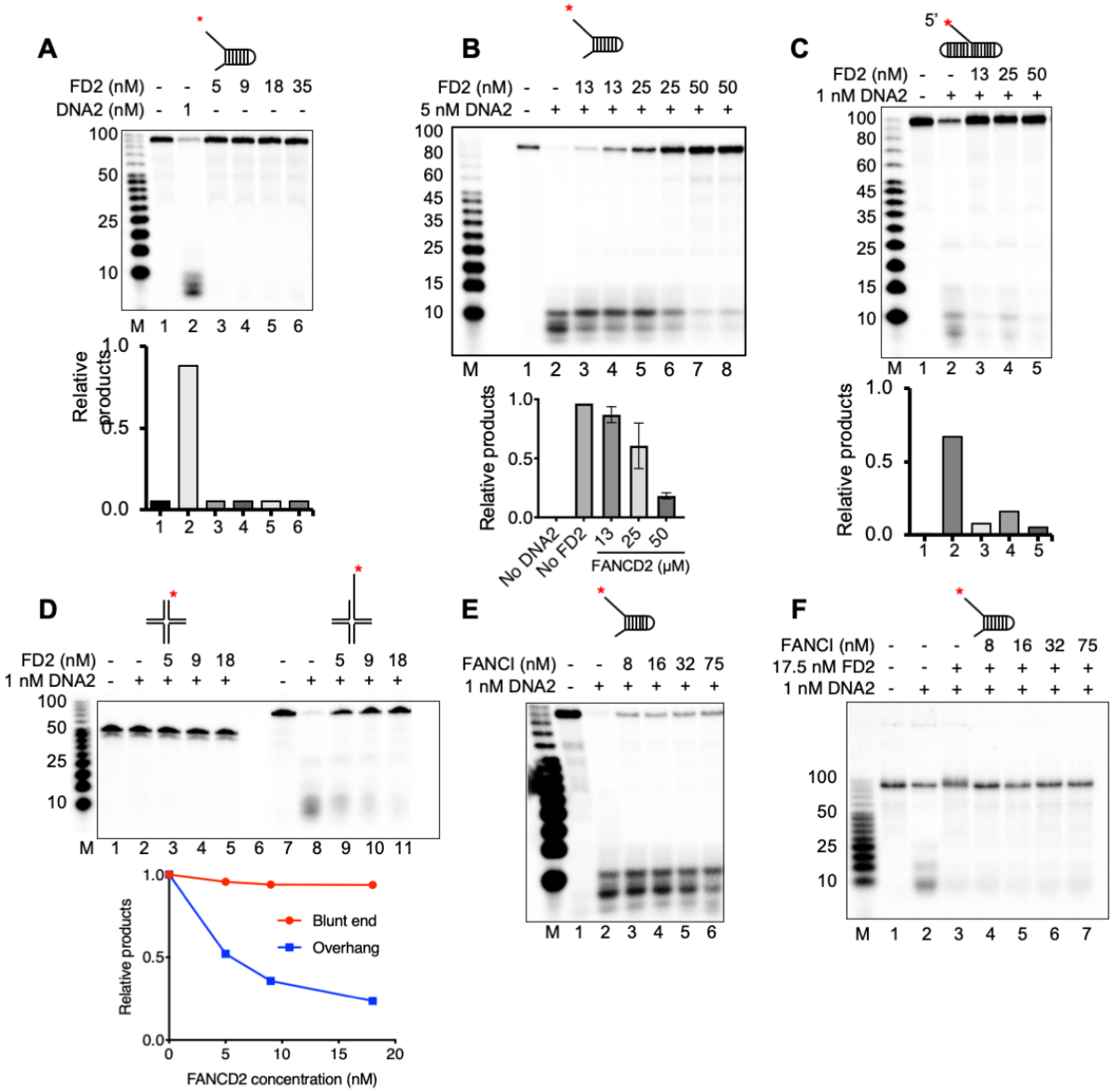
A
FD2 (nM) - - 5 9 18 35
DNA2 (nM) - 1 - - - -
M 1 2 3 4 5 6
Relative products
B
FD2 (nM) - - 13 13 25 25 50 50
5 nM DNA2 - + + + + + + +
M 1 2 3 4 5 6 7 8
Relative products
No DNA2
No FD2
13
25
50
FANCD2 (μM)
C
5'
FD2 (nM) - - 13 25 50
1 nM DNA2 - + + + +
M 1 2 3 4 5
Relative products
D
FD2 (nM) - - 5 9 18 - - 5 9 18
1 nM DNA2 - + + + + - + + + +
M 1 2 3 4 5 6 7 8 9 10 11
Relative products
Blunt end
Overhang
FANCD2 concentration (nM)
E
FANCI (nM) - - 8 16 32 75
1 nM DNA2 - + + + + +
M 1 2 3 4 5 6
F
FANCI (nM) - - - 8 16 32 75
17.5 nM FD2 - - + + + + +
1 nM DNA2 - + + + + + +
M 1 2 3 4 5 6 7
G
FD2 (nM) - - 46 91 91
200 nM MRE11 - + + + -
M 1 2 3 4 5
Relative products
H
FD2 (nM) - - 3 6 11 23 46 91
EXO1 - + + + + + + +
M 1 2 3 4 5 6 7 8

Figure 3. FANCD2 inhibits DNA2 and MRE11 nuclease activities in vitro.

(A) FANCD2 does not show nuclease activity under the conditions of DNA2 nuclease assay, as described in Method Details. Markers show specific DNA2 nuclease product at 10 nt and smaller. Lane 1, DNA substrate without protein; lane 2, DNA2 alone; lanes 3-6, FANCD2 alone.

(B) DNA2 nuclease activity is inhibited by FANCD2-His on a single-stranded fork. Increasing amounts of FANCD2-His were preincubated in DNA2 nuclease reaction (8 μl) mix for 30 min at 4°C. DNA substrate (87 fork, 15 nM, 1 μL) was added, and the reaction was incubated for 30 min at 37°C. All reactions contained equal amounts of FANCD2 diluent. Lane 1, DNA alone; lane 2, DNA2 alone; lanes 3-8, DNA2 (5 nM) plus 13, 25, and 50 nM FANCD2, respectively. Duplicate samples are shown, and quantitation of two separate assays were combined and quantified. In lieu of repeating assays with the additional substrates.

(C-D), Inhibition of DNA2 by FANCD2 on 5' flap substrate (C) and reversed forks (D) (see Figure S5B)). Reactions were as in panel b. Verification of the reversed fork structures is presented in Figure S5B. In lieu of repeating assays with one concentration of DNA2 on the additional substrates, significance was indicated by showing concentration dependence, which is more informative.

(E-F) FANCI does not stimulate inhibition of DNA2 by FANCD2. Reaction conditions were as in panels a-d and FANCI was added at the concentrations indicated at the same time as DNA2.

(G) FANCD2-His inhibits MRE11. FANCD2-His was preincubated in MRE11 nuclease reaction mix on ice for 30 min.

(H) FANCD2 does not inhibit EXO1. FANCD2 was added as indicated.

Figure 4

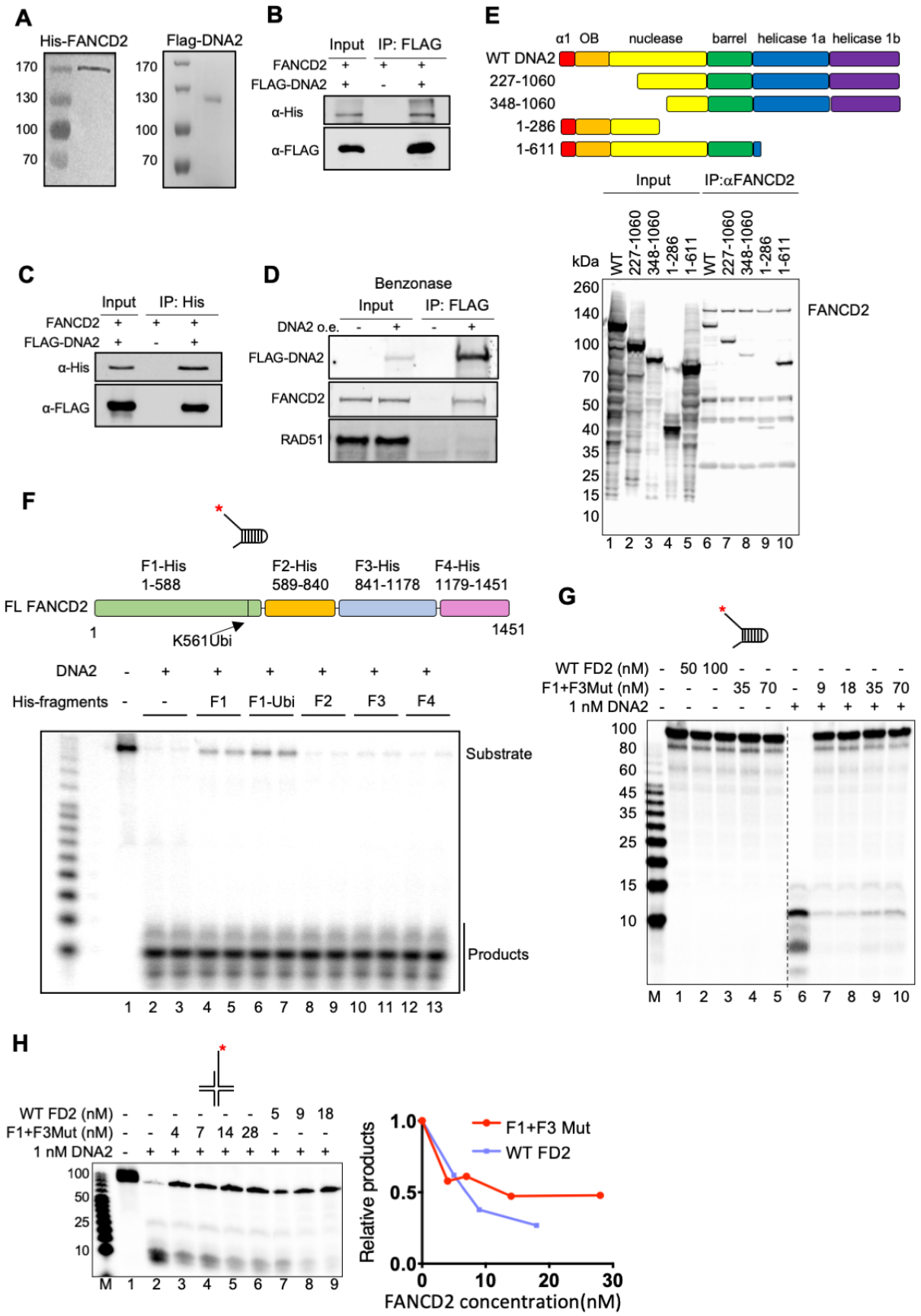
A
His-FANCD2
Flag-DNA2
170
130
100
70
B
Input
IP: FLAG
FANCD2
FLAG-DNA2
α-His
α-FLAG
C
Input
IP: His
FANCD2
FLAG-DNA2
α-His
α-FLAG
D
Benzonase
Input
IP: FLAG
DNA2 o.e.
FLAG-DNA2
FANCD2
RAD51
E
α1
OB
nuclease
barrel
helicase 1a
helicase 1b
WT DNA2
227-1060
348-1060
1-286
1-611
Input
IP:αFANCD2
kDa
WT
227-1060
348-1060
1-286
1-611
FANCD2
260
140
100
70
50
40
35
25
15
10
1 2 3 4 5 6 7 8 9 10
F
F1-His
1-588
F2-His
589-840
F3-His
841-1178
F4-His
1179-1451
FL FANCD2
1
K561Ubi
1451
DNA2
His-fragments
F1
F1-Ubi
F2
F3
F4
Substrate
Products
1 2 3 4 5 6 7 8 9 10 11 12 13
G
WT FD2 (nM)
F1+F3Mut (nM)
1 nM DNA2
100
80
60
45
35
25
15
10
M 1 2 3 4 5 6 7 8 9 10
H
WT FD2 (nM)
F1+F3Mut (nM)
1 nM DNA2
100
50
25
10
M 1 2 3 4 5 6 7 8 9
Relative products
1.0
0.5
0.0
0
10
20
30
FANCD2 concentration(nM)
F1+F3 Mut
WT FD2

Figure 4. FANCD2/DNA2 interaction and FANCD2/DNA contributions to DNA2 nuclease inhibition.

(A) Purified FANCD2-His and FLAG-DNA2. Proteins were purified as described in Method Details and analyzed by SDS gel.

(B) FANCD2 and DNA2 interact in vitro. FLAG-DNA2 was over expressed in 293T cells, and purified by binding to M2 FLAG beads. The beads were washed with lysis buffer and then incubated with purified FANCD2 protein (1 μg/ml) at 4°C for 1 h. Beads were washed with PBS 5 times and then in 2XSDS loading buffer followed by western blotting. Empty M2 beads incubated with FANCD2 served as negative control.

(C) FLAG-DNA2 is immuno-precipitated by His-tagged FANCD2 in vitro. 1 μg/ml DNA2 protein was incubated with FANCD2-His bound to Ni-NTA beads at 4°C for 1 hour. Beads were washed 5 times with PBS, and then boiled in 2XSDS loading buffer for western blotting. Empty Ni-NTA beads were incubated with FLAG-DNA2 as negative control.

(D) FLAG-DNA2 was over expressed in wild type U2OS cells, and nuclear extract was prepared; Benzonase was added to remove DNA. FLAG-DNA2 was pulled down with M2-beads. The beads were washed with nuclear preparation buffer and eluted with FLAG peptide. The elution was prepared for immunoblot. See Method Details.

(E) FANCD2 interacts with the N terminal domain of DNA2. (Top) Map of DNA2 domains and truncations of DNA2. (Bottom) Coimmunoprecipitation of the DNA2 mutant proteins using a FANCD2 antibody. Cell lysates with overexpressed FLAG-DNA2 protein were supplemented with 2 nM FLAG-FANCD2. Pull-down was performed using FANCD2 antibody. Products were separated using SDS-PAGE and imaged by western blot analysis using 3XFLAG antibody. revealing both FANCD2, as indicated, and DNA2 full length and deletion proteins.

(F) Mapping of the FANCD2 inhibitory domain. DNA2 nuclease assays were performed as in Figure 3 using the FANCD2 fragments indicated (Niraj et al., 2017). Assays were performed in duplicate using 0.2 nM DNA2 and 30 nM FANCD2 and were repeated four times.

(G) Inhibition of hDNA2 by the hFANCD2-F1+F3Mut DNA binding mutant protein – 87 fork substrate. Conditions were as in Figure 3A except that mutant FANCD2 was used. Lanes 1-5, FANCD2 wild type (WT) and F1+F3Mut alone, lane 6, DNA2 (1 nM) alone; lanes 7-10, DNA2 (1 nM) plus 9, 18 35, and 70 nM FANCD2-F1+F3Mut protein, respectively.

(H) Inhibition of hDNA2 by the hFANCD2-F1+F3Mut DNA binding mutant protein – reversed fork substrate.

Figure 5

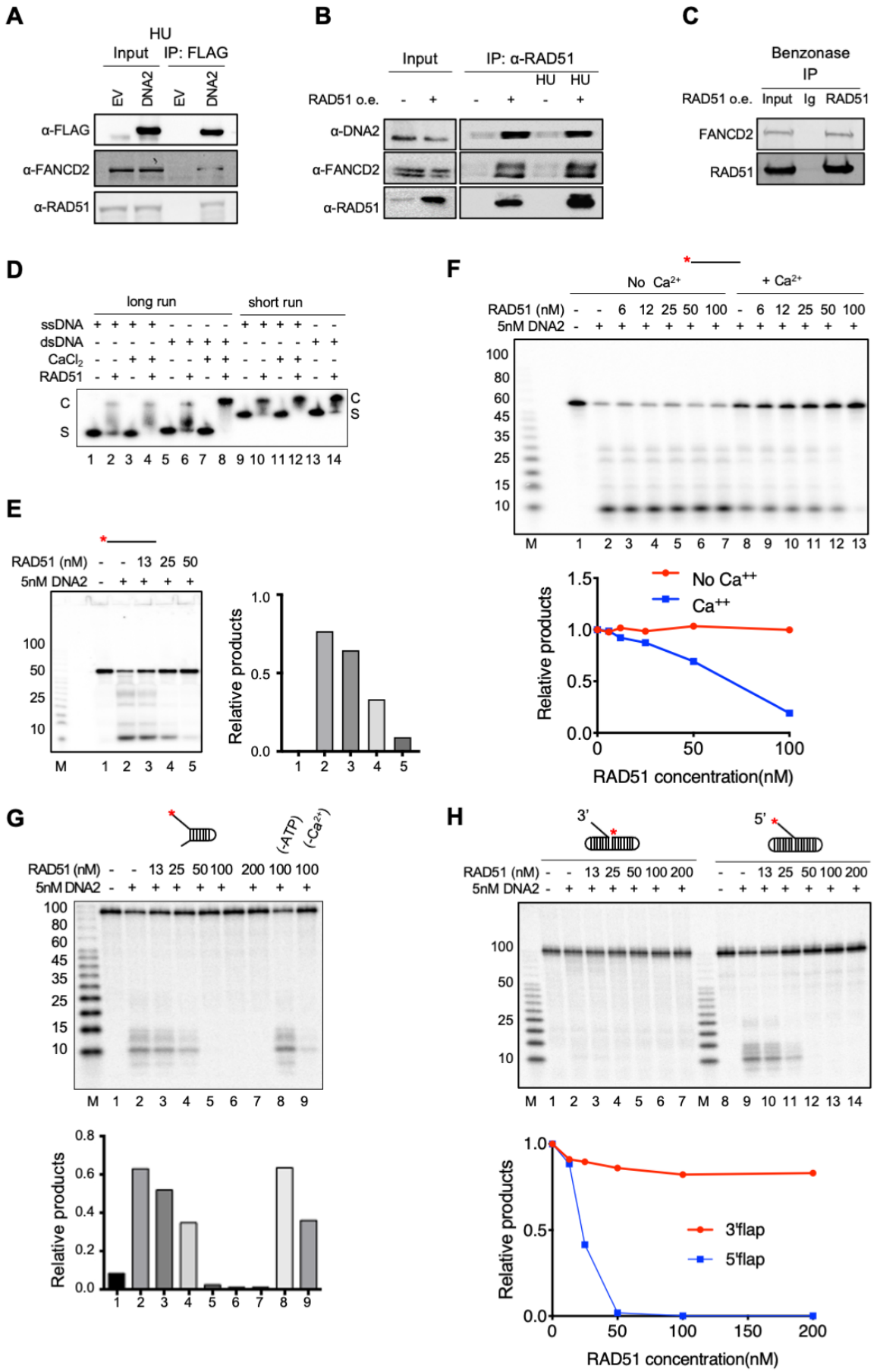
A
HU
Input
IP: FLAG
EV
DNA2
EV
DNA2
α-FLAG
α-FANCD2
α-RAD51
B
Input
IP: α-RAD51
HU
HU
RAD51 o.e.
α-DNA2
α-FANCD2
α-RAD51
C
Benzonase
IP
RAD51 o.e.
Input
Ig
RAD51
FANCD2
RAD51
D
long run
short run
ssDNA
dsDNA
CaCl2
RAD51
C
S
1 2 3 4 5 6 7 8 9 10 11 12 13 14
E
RAD51 (nM)
5nM DNA2
Relative products
F
No Ca2+
+ Ca2+
RAD51 (nM)
5nM DNA2
M
No Ca++
Ca++
Relative products
RAD51 concentration(nM)
G
(-ATP)
(-Ca2+)
RAD51 (nM)
5nM DNA2
Relative products
H
3'
5'
RAD51 (nM)
5nM DNA2
3'flap
5'flap
Relative products
RAD51 concentration(nM)

Figure 5. RAD51 filaments protect DNA from DNA2 mediated degradation.

(A) Co-immunoprecipitation of FANCD2 and RAD51 (FLAG-DNA2 pull-down). FLAG-tagged DNA2 or empty vector was transfected into A549 cells, 24 hours later cells were treated with 2 mM HU for 3 hours and then harvested. Cells were lysed and pull down carried out with FLAG M2 beads; the beads were washed with lysis buffer then boiled with SDS loading buffer; immunoprecipitates were analyzed by western blotting of a 12% acrylamide gel with the indicated antibodies.

(B) Co-immunoprecipitation of FANCD2 and RAD51 using RAD51 antibody for immunoprecipitation. RAD51 vector or empty vector was transfected into 293T cells and cells were split 24 hours post-transfection. At 48 hours post-transfection, cells were incubated with or without 2 mM HU for 3 hours; cells were then harvested and lysed. Lysates were incubated with RAD51 antibody and IgG-agarose beads, then washed with lysis buffer. Immunoprecipitates were analyzed for FANCD2 and DNA2 by western blotting on an 8% acrylamide gel.

(C) RAD51 and FANCD2 interact in the absence of DNA. U2OS cell nuclear extract was prepared as described in Method Details. Extracts were treated with Benzonase. 10ul RAD51 antibody or IgG control added to 50μg nuclear extract and incubated for 1 hour at 4°C. 10ul Protein A agarose beads added then incubated for 1 hour at 4°C. The beads were washed with nuclease buffer and boiled with SDS sample buffer for western blot.

(D) Ca^{2+} enhances DNA binding activity of RAD51. 1 nM ssDNA or dsDNA was incubated in a 10 μl reaction mixture containing 200 nM RAD51, 25 mM TrisOAc (pH 7.5), 1 mM $MgCl_2$, 2 mM $CaCl_2$ and 2 mM ATP (except where $CaCl_2$ was omitted), 1 mM DTT, 0.1 BSA mg/ml, as indicated. The reaction was incubated for 10 min at 37°C(Wang et al., 2015) and samples were mixed with 1 μl loading buffer (2.5%Ficoll-400, 10 mM Tris-HCl, pH 7.5 and 0.0025% xylene cyanol). Products were analyzed on a 5% native gel (29:1 30% acrylamide in TAE), constant voltage, 60V, in the cold room for 1h (lanes 9-14) or 2h (lanes 1-8) followed by phosphor imaging.

(E-F) RAD51 filaments inhibit DNA2 on a ssDNA substrate. Increasing amounts of RAD51 were preincubated with 4 nM ssDNA (JYM945) in 25 mM TrisOAc (pH 7.5), 2 mM $MgCl_2$, 2 mM $CaCl_2$, 2 mM ATP, 0.1 mg/ml BSA, and 2 mM DTT for 10 min at 37°C, conditions shown to be permissive for both filament formation and DNA2 nuclease activity in control assays (not shown). DNA2 was then added to 5 nM as indicated and reactions incubated for 30 min at 37°C. Samples were processed, run on a sequencing gel and analyzed by image J. Ca^{2+} (2 mM) was present in panel e and in the indicated lanes of panel F.

(G) RAD51 filaments inhibit DNA2 on the forked substrate- 87 fork. Increasing amounts of RAD51 were preincubated with 4 nM 87 fork substrate prior to the addition of DNA2 as described in panels e-f. Controls show DNA2 activity in the presence of 100 nM RAD51 and in the absence of ATP (lane 8) or Ca^{2+} (lane 9).

(H) RAD51 filaments inhibit DNA2 on a 5’ or 3’ flap. The indicated amounts of RAD51 were incubated with 4 nM of the respective flap substrate prior to the addition of DNA2 as described in panels e-g.

Figure 6

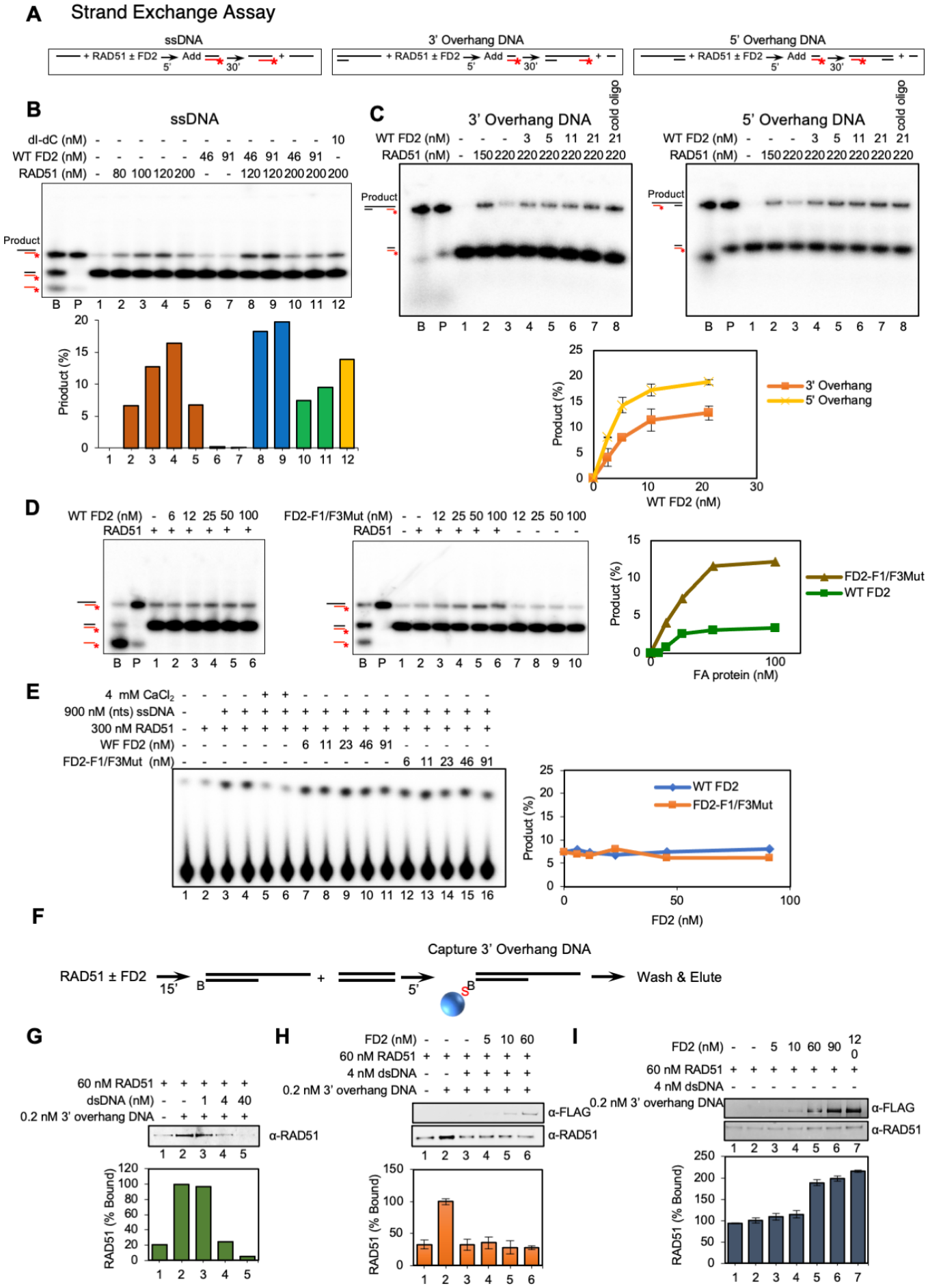
A
Strand Exchange Assay
ssDNA
3' Overhang DNA
5' Overhang DNA
+ RAD51 ± FD2
Add
5'
30'
B
ssDNA
dI-dC (nM)
WT FD2 (nM)
RAD51 (nM)
Product
Prioduct (%)
C
3' Overhang DNA
5' Overhang DNA
cold oligo
Product (%)
WT FD2 (nM)
3' Overhang
5' Overhang
D
WT FD2 (nM)
RAD51
FD2-F1/F3Mut (nM)
FD2-F1/F3Mut
WT FD2
FA protein (nM)
E
4 mM CaCl2
900 nM (nts) ssDNA
300 nM RAD51
WF FD2 (nM)
FD2-F1/F3Mut (nM)
FD2 (nM)
F
Capture 3' Overhang DNA
RAD51 ± FD2
15'
5'
Wash & Elute
G
60 nM RAD51
dsDNA (nM)
0.2 nM 3' overhang DNA
α-RAD51
RAD51 (% Bound)
H
FD2 (nM)
60 nM RAD51
4 nM dsDNA
0.2 nM 3' overhang DNA
α-FLAG
α-RAD51
I
FD2 (nM)
60 nM RAD51
4 nM dsDNA
0.2 nM 3' overhang DNA
α-FLAG
α-RAD51

Figure 6 FANCD2 stimulates RAD51-mediated strand exchange.

(A) Schematic of strand exchange assay: Single-stranded or 3' or 5' overhang DNA is incubated in the presence of RAD51 to form filaments. The filaments are then incubated with a duplex DNA with a labeled strand complementary to the filament. Product formation, representing complete strand exchange, is monitored using a native acrylamide gel.

(B) FANCD2 stimulates strand exchange on ssDNA by high levels of RAD51. Quantification is shown below each gel. Lane labeled B shows the migration of each relevant DNA species as indicated in the schematic on the left and was prepared by annealing oligonucleotide EXTJYM925, JYM925, and 5' labeled JYM945; The lane labeled P confirms the position of the exchanged strand product (EXTJYM925 and 5' labeled JYM945). Lanes 1-5: 4 nM ssDNA (100 nt, oligonucleotide EXTJYM925) was incubated with indicated amounts of RAD51 for 5 min at 37˚C and the 5' labeled dsDNA (60mer, JYM925/JYM945 oligonucleotides) (final concentration 4 nM) was added and incubation continued for an additional 30 min at 37˚C for strand exchange. Lanes 6 and 7, as in lanes 1-5 with indicated concentrations of FANCD2 in the absence of RAD51. Lanes 8-11: RAD51 plus FANCD2 at the indicated concentrations present during both the 5' preincubation with ssDNA and after addition of dsDNA. Lane 12: 10 nM of dI-dC competitor present during preincubation of RAD51 and ssDNA. Histogram shows quantitation.

(C) FANCD2 stimulates strand exchange on 3' and 5' overhang DNA by high levels of RAD51. Reactions performed as in panel B) however, 4 nM 3' overhang DNA (162 nt RJ-167 annealed to 42 nt RJ-PHIX-42-1) (Left) or 4 nM 5' overhang DNA (162 nt RJ-167 annealed to 42 nt RJ-PHIX-42-2) (Right) as indicated, were incubated in the presence of indicated amounts of RAD51 for 5 min at 37˚C to form filaments. 5' labeled dsDNA (40mer, RJ-Oligo1/RJ-Oligo2 in the case of 3' overhang DNA or RJ-Oligo4/RJ-Oligo3 in the case of 5' overhang DNA) (final concentration 4 nM) was added and incubation continued for an additional 30 min at 37˚C for strand exchange. Lanes 1, no protein; lanes 2-3: RAD51 alone; lanes 4-7: RAD51 plus FANCD2 at the indicated concentrations present during both the 5' preincubation with 3' or 5' overhang DNA and after addition of dsDNA. Lane 8: 10-fold excess of unlabeled heterologous ssDNA (40 nt, oligonucleotide RJ-Oligo2) complementary to labeled strand of dsDNA was added to the stop solution to rule out that the product observed was due to denaturation and annealing during the deproteinization/termination step. (% Product represents the value with unstimulated exchange subtracted.) The graph shows quantification for both assays. The assays were repeated twice.

(D) Wild-type FANCD2 and FANCD2-F1-F3Mut stimulate strand exchange. Parallel reactions were carried out with WT or mutant and run on separate gels. Left: Lanes 1-6 (left): Titration of WT FANCD2 at 100 nM RAD51 and 2 nM of both ssDNA and dsDNA. Assays were performed with oligonucleotides as in panel b. Right: lanes 2-10 (right): Indicated amounts of mutant FANCD2 incubated in the absence of RAD51 during both the preincubation with

ssDNA and after addition of dsDNA. Graph shows quantification for both assays.

(E) Wild-type and mutant FANCD2 do not inhibit RAD51 ATPase.

(F) Schematic of biotinylated DNA pull-down assay: B-biotin; S-streptavidin.

(G) Assembly of RAD51 onto 3' overhang DNA is suppressed by heterologous dsDNA competitor. RAD51 and FANCD2 proteins at indicated concentrations were incubated for 15 min at 37˚C followed by the addition of 3' overhang DNA (162 nt RJ-167 annealed to 42 nt 3' Bio-RJ-PHIX-42-1) and competitor heterologous dsDNA (90mer, Oligo #90/Oligo #60 oligonucleotides) and incubated for an additional 5 min at 37˚C. Where DNA was omitted, TE buffer was used and similarly, respective proteins storage buffers were used where proteins were omitted. 20 µL reactions were performed as in panel f using 60 nM RAD51 either in the absence (lane 2) or presence (lanes 3-5) of excess competitor heterologous dsDNA (90mer, Oligo#90/Oligo#60 oligonucleotides). Histogram shows quantification. Assays were repeated two times.

(H) FANCD2 does not rescue RAD51 filament formation on 3' overhang DNA in the presence of heterologous dsDNA competitor. 20 µL reactions were performed as in panel F using 60 nM RAD51 preincubated with (lanes 3-6) or without (lane 2) increasing concentrations of FANCD2. Both proteins were separately probed by western analysis. The histogram shows quantification of the RAD51 western analysis. Assays were repeated two times.

(I) FANCD2 stimulates RAD51 filament formation on 3' overhang DNA in the absence of dsDNA competitor. Reactions were performed as in panel f using 60 nM RAD51 preincubated with (lanes 3-7) or without (lane 2) increasing concentrations of FANCD2. TE Buffer in lieu of dsDNA was added with 3' overhang DNA for all samples and incubated for an additional 5 min at 37˚C. Both proteins were separately probed for western blot analysis. Histogram shows quantification of the RAD51 western blot analysis. Assays were repeated two times.

Figure 7

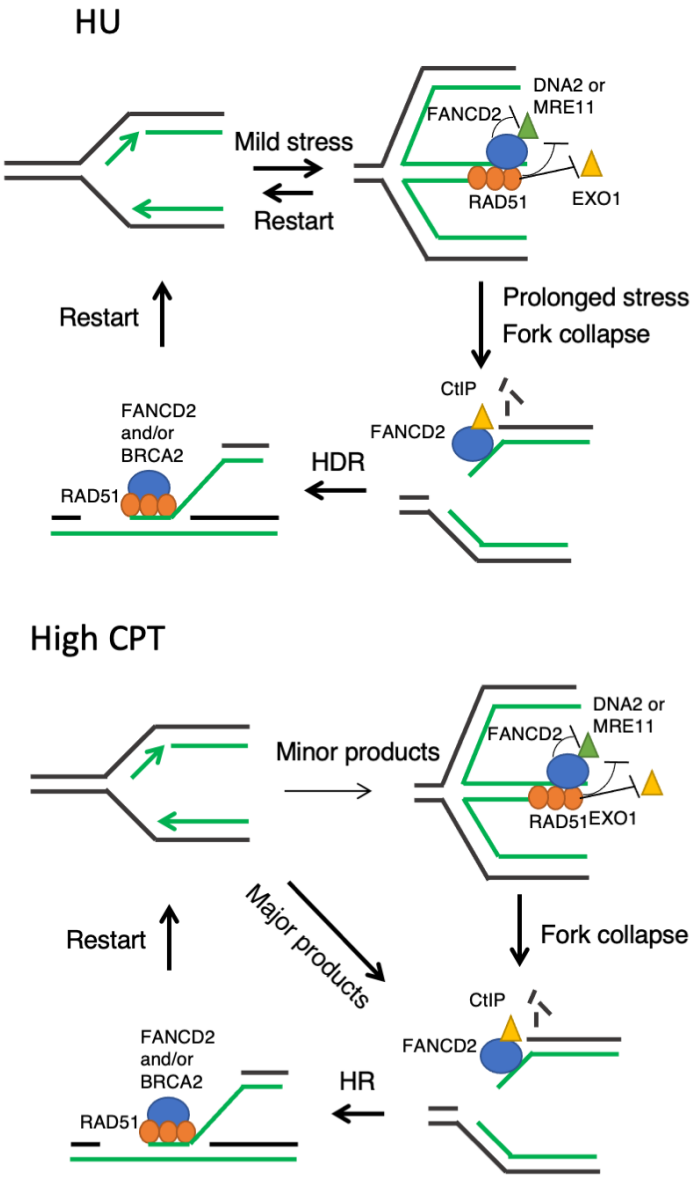
HU
Mild stress
Restart
DNA2 or
MRE11
FANCD2
RAD51
EXO1
Restart
Prolonged stress
Fork collapse
CtIP
FANCD2
FANCD2
and/or
BRCA2
RAD51
HDR
High CPT
Minor products
DNA2 or
MRE11
FANCD2
RAD51
EXO1
Restart
Major products
Fork collapse
CtIP
FANCD2
FANCD2
and/or
BRCA2
RAD51
HR

Figure 7. Model for multiple roles of FANCD2 in fork protection studied in this work

At a stalled replication fork reversed upon moderate stress, FANCD2 can protect the regressed arm by directly inhibiting DNA2 or stabilizing RAD51 on the ssDNA to prevent digestion by various various nuclease. In prolonged stress or at CTP induced damage, FANCD2 can recruit CtIP to the broken fork to facilitate resection and HDR. FANCD2 may also promote RAD51 mediated strand exchange reactions to restart fork either together with BRCA2 or by itself.